these modalities, it remains difficult to increase the temperature of only the cancer tissues in a controlled manner without damaging surrounding normal tissues.

More than 40,000 people are diagnosed with oral cancer, including cancers of the mouth, tongue, tonsils, and throat, every year in the US alone. Oral cancer can cause functional damage and disfigurement, and, in its advanced stages, it invades surrounding organs, causing disorders of speech, swallowing, and even chewing. Surgery may have serious adverse effects, so chemotherapy or radiation therapy is often favored in oral cancer patients, not with standing potentially serious systemic side effects. Hyperthermia is often preferred, e.g., for metastatic N3 cervical lymph nodes, because it has fewer adverse side effects. However, it is difficult to induce hyperthermia in a metastatic node-specific manner. Nevertheless, selective hyperthermia has been studied as a possible approach to obtain tumor-specific cytotoxicity, e.g., by ferromagnetic embolization [7]. More recently, magnetic nanoparticles (MNPs) have been investigated for this purpose, because MNPs generate heat when they are exposed to an alternating magnetic field (AMF) as a result of hysteresis and relaxational losses [8].

Ferucarbotran (Resovist®) is an organ-specific contrast agent used in magnetic resonance imaging (MRI) of local tumors, and the permissible dose in humans has been established by at least two studies [9, 10]. Because ferucarbotran consists of superparamagnetic iron oxide (SPIO) coated with carboxydextran, it generates heat when it is exposed to an AMF [11, 12], and it has been reported to induce selective hyperthermia when used in arterial embolization [11]. However, it has not been established whether ferucarbotran is suitable for inducing hyperthermia in cancer treatment.

Cisplatin (*cis*-diaminedichloroplatinum II; CDDP) is widely used in chemotherapy in many types of cancer, including oral cancers [13]. However, it has serious side effects, including acute kidney damage and/or renal failure [14–16]. Recent studies have demonstrated that hyperthermia stimulates cellular uptake of cisplatin [17, 18] and consequently enhances the cytotoxicity of cisplatin in cancer cells, both in vitro and in vivo [19–21]. Thus, combined treatment with cisplatin plus hyperthermia may allow the effective dose of cisplatin to be decreased sufficiently to minimize serious side effects.

Accordingly, in order to examine the feasibility of using combination therapy with cisplatin and ferucarbotran/AMF-induced hyperthermia in the therapy of oral cancer, in this study we examined the effect of the combined treatment on oral cancer cells in culture. Our results confirmed that ferucarbotran/AMF-induced hyperthermia significantly enhances the effect of cisplatin. Because both cisplatin and ferucarbotran have already been approved for clinical use, early introduction of this technique, at least for oral cancers, should be feasible.

## Materials and methods

### Reagent, drug and cell lines

Ferucarbotran (Resovist®) was purchased from FUJIFILM Pharma (Tokyo, Japan) [11]. Cisplatin was purchased from Wako Pure Chemical Industries (Osaka, Japan). Human oral squamous cell carcinoma cell lines OSC-19 and HSC-3 were purchased from the Japan Health Sciences Foundation, Health Science Research Resources Bank (Osaka, Japan). In all cases, cells from early passage cultures were stored and used for the experiments. OSC-19 and HSC-3 were cultured in Dulbecco's modified Eagle's medium (DMEM), 1 % penicillin–streptomycin, and 1 % L-glutamine.

### Thermography

Thermal images were taken using a thermograph (infrared thermal imaging camera InfReC R300SR; Nippon Avionics, Tokyo, Japan). Temperature was also measured using a thermograph.

### Alternating magnetic field (AMF) generator

An AMF was generated by a vertical coil with an inner diameter of 6.5 cm, driven by a transistor inverter (HOT SHOT; Ameritherm, New York, USA) operated at a

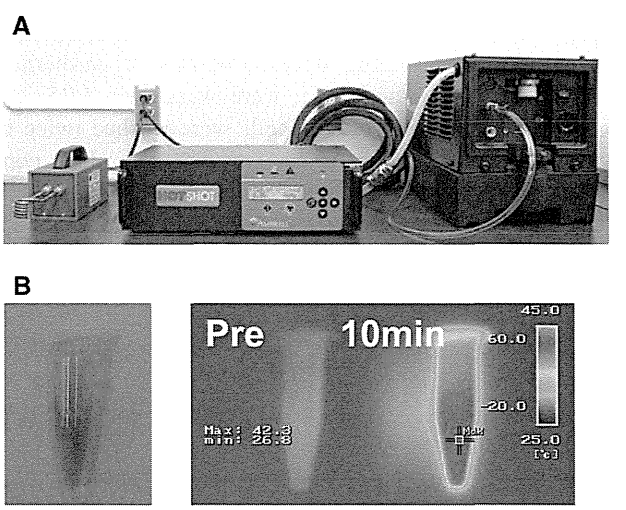


**Fig. 1** Heat generation by ferucarbotran in an alternating magnetic field (AMF). **a** The alternating magnetic field (AMF) generator, **b** a photograph of ferucarbotran in medium (*left*), and thermal images of ferucarbotran in medium before (*middle*), and 10 min after AMF (308 kHz, EC 270 A) (*right*)

frequency of 308 kHz and electric current (EC) 250 A [12, 22–26]. Temperature was measured using a hand-held thermometer, HA-200 (Anritsu Meter, Tokyo, Japan).

### Apoptosis assay

HSC-3 cells and OSC-19 ($6 \times 10^4$ cells/well) were seeded on 6-cm dishes and incubated for 24 h. Cisplatin was then added to a concentration of 0 μM (control), 7.5 or 15 μM. When hyperthermia was to be applied, 10 mM ferucarbotran was added and AMF was performed with a HOT SHOT under the conditions described above [22, 25, 26]. Incubation was continued for 12 h at 37 °C, in an atmosphere of 5 % $CO_2$ in air. Cells were washed twice with cold PBS and suspended in 1× binding buffer at a concentration of $1 \times 10^6$ cells/ml. Next, a 100-μl aliquot of the solution, containing $1 \times 10^5$ cells, was transferred to a 5-ml culture tube. Then, 5 μl of allophycocyanin (APC) Annexin V and 5 μl of 7-aminoactinomycin D (AAD) (BD Biosciences, CA, USA) [27] were added to the tube. Incubation was continued for 15 min at room temperature (25 °C) in the dark. Finally, 400 μl of 1× binding buffer were added to each tube. Cells were examined by flow cytometry (BD FACSCanto II; BD Biosciences).

### Cell cycle analysis

Cell cycle analysis was performed using The Cycletest$^{TM}$ Plus DNA Reagent Kit (BD Biosciences) according to the manufacturer's protocol [28]. Briefly, HCS-3 and OSC-19 cells treated with 0 μM (control), 7.5 or 15 μM cisplatin, with or without hyperthermia (10 mM ferucarbotan/AMF), were washed in PBS and fixed in 90 % ethanol. Fixed cells were washed twice in PBS and stained with 50 μM propidium iodide containing 5 μg/ml DNase-free RNase for 1 h, then analyzed by flow cytometry using a FACScan (BD FACSCanto II).

### Statistical analysis

Data were analyzed using BD FACSDiva software (BD Biosciences). Data are expressed as mean ± SEM. Data were analyzed by one-way ANOVA followed by the Tukey post hoc test using GraphPad Prism software (GraphPad Software, CA, USA). The criterion of statistical significance was set at $p < 0.05$.

## Results

### Heat generation by ferucarbotran in an alternating magnetic field (AMF)

Heat production is determined by the magnetic properties of ferucarbotran, its concentration, and the strength of the AMF [12]. Therefore, we examined the heating effect of AMF on medium containing ferucarbotran by thermography (Fig. 1b). As shown in Fig. 2, the temperature increased time-dependently, and the extent of the increase was dependent on the concentration of ferucarbotran (Fig. 2a) and the magnitude of the EC used to generate AMF (Fig. 2b). The results showed that AMF produced at

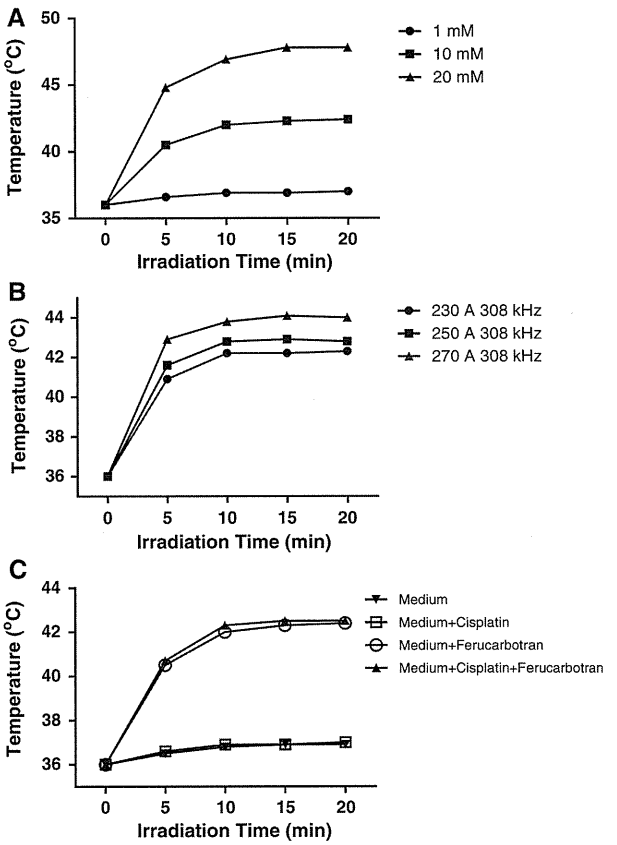


**Fig. 2** Dependence of heat generation on ferucarbotran concentration and alternating magnetic field (AMF) strength. **a** Temperature–time curves at different concentrations of ferucarbotran (1, 10, or 20 mM equivalent of iron) on AMF at 308 kHz and EC 230 A. **b** Temperature–time curves in the presence of 10 mM ferucarbotran on AMF at different levels of electric current (230–270 A) at 308 kHz. **c** Effect of cisplatin (30 μM) on ferucarbotran (1, 10, or 20 mM equivalent of iron)/AMF (308 kHz, EC 230 A)-induced increase of temperature; medium only, medium + cisplatin, medium + ferucarbotran, and medium + cisplatin + ferucarbotran

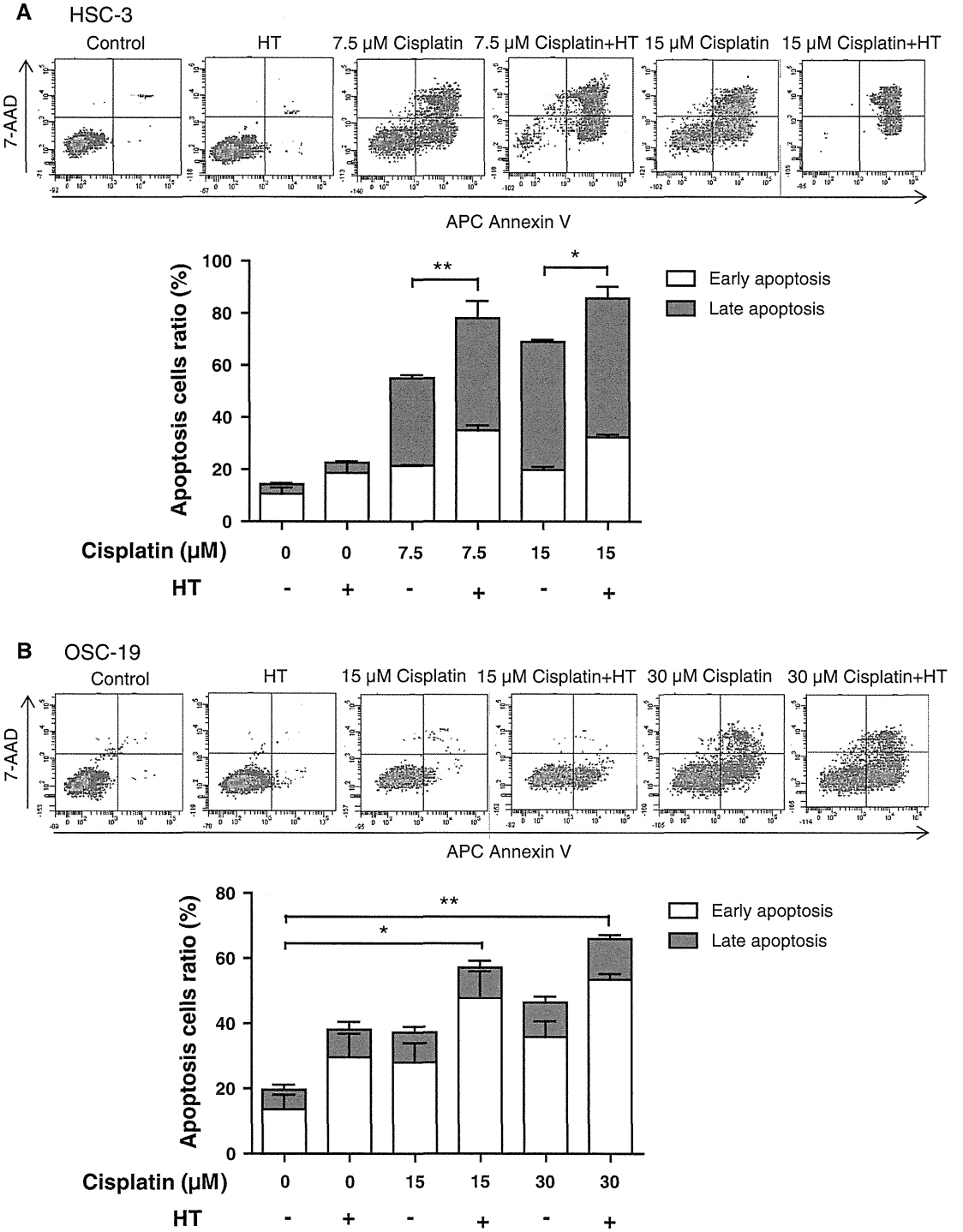


**Fig. 3** Ferucarbotran/AMF-induced hyperthermia enhances the pro-apoptotic effect of cisplatin in human oral cancer cells. Annexin-V/PI staining of human oral cancer cells at 12-h intervals after treatment with 0, 7.5, or 15 μM cisplatin with or without hyperthermia (HT) in HSC-3 cells, and 0, 15, 30 μM cisplatin with or without HT in OSC-19 cells. **a** Representative analysis of apoptosis of HCS-3 cells and OSC-19 cells exposed to cisplatin and ferucarbotran with or without AMF. Annexin-V/PI method with FACS scan dot plot analysis was used to divide the treated and control cells into four groups: (1) living cells (*lower left quadrant*); (2) necrotic cells (*upper left quadrant*); (3) early apoptotic cells (*lower right quadrant*); and (4) late apoptotic cells (*upper right quadrant*). **b** Representative analysis of apoptosis of OSC-19 cells exposed to cisplatin with or without AMF. $*p < 0.05$, $**p < 0.01$; $n = 4$

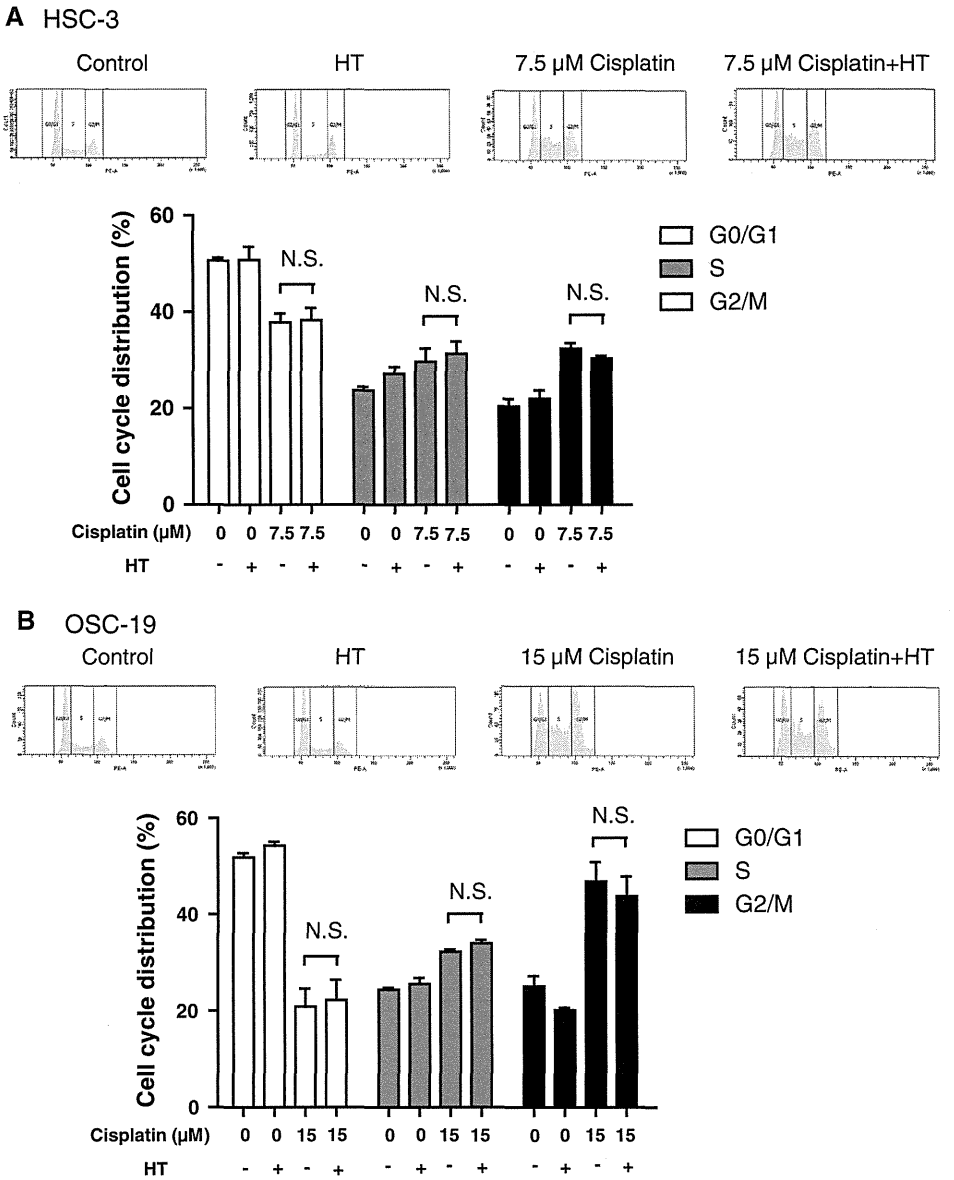


**Fig. 4** Combination of cisplatin and ferucarbotran/AMF-induced hyperthermia causes G2/M arrest. Cell cycle analysis of HSC-3 and OSC-19 cells at 48-h intervals after treatment with 0, 7.5, or 15 μM of cisplatin with or without hyperthermia (HT). **a** Representative cell cycle analysis of HSC-3 cells in response to cisplatin treatment with or without AMF (*upper panel*) and of OSC-19 cells in response to cisplatin treatment with or without AMF (*lower panel*). *NS* not significant; $n = 4$

generator settings of 308 kHz and EC 250 A in the presence of 10 mM (equivalent of iron) ferucarbotran was sufficient to generate a temperature of 42.5 °C, and we adopted these conditions for the subsequent assays. We confirmed that cisplatin did not alter the heating effect under these conditions (Fig. 2c).

## Ferucarbotran-enhanced cisplatin-mediated apoptosis

It has been reported that cisplatin induces apoptosis in cancer cells [29]. We thus examined whether ferucarbotran/AMF-induced hyperthermia further increased cisplatin-induced apoptosis in oral cancer cells. FACS analysis demonstrated that cisplatin increased both early and late apoptosis in a dose-dependent manner in HSC-3 cells (Fig. 3a) and OSC-19 cells (Fig. 3b). Ferucarbotran/AMF-induced hyperthermia for an hour significantly increased the apoptotic effect of cisplatin.

## Cisplatin-induced G2/M arrest of human oral cancer cells was unaffected by hyperthermia

To examine whether hyperthermia modifies the mechanism of anti-cancer action of cisplatin, flow-cytometric cell-cycle analysis of treated cells was performed. Cisplatin induced potent G2/M arrest in both HSC-3 cells (Fig. 4a) and OSC-19 cells (Fig. 4b). We found that ferucarbotran/AMF-induced hyperthermia did not alter the effect of

cisplatin on the cell cycle. Thus, hyperthermia per se had no effect on the anti-cancer mechanism of cisplatin.

## Discussion

Ferucarbotran is an organ-specific superparamagnetic contrast agent used in MRI, and its safety and maximum dosage (10 mM; 0.016 mL/kg, which contains 8 μmol (0.45 mg) Fe/kg equivalent of iron [30]) have been well established [9, 10]. Since hyperthermia has already been shown to enhance the anti-cancer effect of cisplatin [31] in the treatment of oral cancer, we anticipated that combination therapy with cisplatin and ferucarbotran/AMF-induced hyperthermia might be suitable for oral cancer treatment, making it possible to reduce the necessary dose of cisplatin and consequently reduce the risk of serious side effects.

Hyperthermia to induce apoptosis of cancer cells is best performed at about 42 °C, because temperatures above 44 °C have been reported to cause necrosis and damage to surrounding normal tissues [32]. Therefore, we first confirmed that the above concentration of ferucarbotran was sufficient to maintain a temperature of 42.5 °C under appropriate AMF conditions, and this level of hyperthermia could induce apoptosis of oral cancer cells, as evaluated by FACS analysis. It should be noted that it would still be necessary to optimize AMF conditions for clinical treatment. Similarly, it would be desirable to deliver cisplatin and ferucarbotran to oral cancer tissue in a selective manner. This may be achieved by the use of superselective intra-arterial infusion with a catheter, as we previously reported in oral cancer patients [33].

We previously reported that ROS production was higher in cancer cells than in normal cells, and was further increased when the temperature was increased [34]. Cisplatin also increases ROS production, and this is most likely the mechanism responsible for its anti-cancer effect [34, 35]. We confirmed that the combination of cisplatin and ferucarbotran/AMF-induced hyperthermia further enhanced ROS production (data not shown). This is important, because cisplatin may cause ototoxicity [36], so it is desirable to minimize the necessary cisplatin dose, as far as is consistent with therapeutic effectiveness, in the clinical context.

It is well known that cisplatin causes accumulation of cells in S phase and blocks the G0/G1 phases in xenografted human head and neck carcinoma cells [37], leading to apoptosis. [38, 39]. Our data showed that ferucarbotran/AMF-induced hyperthermia enhanced the anti-cancer effect of cisplatin without altering its characteristic effect on the cell cycle. Accordingly, ferucarbotran/AMF-induced hyperthermia did not appear to modify the mechanism of action of cisplatin in human oral cancer cells. Because both cisplatin and ferucarbotran are already in clinical use, we believe the combination of cisplatin with ferucarbotran/AMF-induced hyperthermia has the potential for early clinical application. It should at least be possible to reduce the clinically effective dosage of cisplatin by administering it in combination with ferucarbotran/AMF, thereby reducing the risk of serious cisplatin-related side effects. Further investigation seems warranted to confirm the safety and effectiveness of this combined treatment for oral cancers in humans.

**Acknowledgments** The authors are grateful to Akane Nagasako for technical assistance in this study. This work was supported in part by the Japan Society for the Promotion of Science (JSPS) (IS), as well as a Grant-in-Aid for JSPS Fellows (I.S.) from the Ministry of Health, Labor and Welfare of Japan (Y.I.), a Grant-in-Aid from the New Energy and Industrial Technology Development Organization of Japan (NEDO) (Y.I.), a Grant-in-Aid for Scientific Research on Innovative Areas (22136009) (Y.I.) from the Japanese Ministry of Education, Culture, Sports, Science, and Technology of Japan (Y.I.), a grant from the IHI Corporation (H.E.), and a Grant for a Research and Development Project of Yokohama City University (Y.I.).

**Conflict of interest** The authors declare no potential conflicts of interest.

## References

1. van der Zee J (2002) Heating the patient: a promising approach? Ann Oncol 13(8):1173–1184
2. Abe M, Hiraoka M, Takahashi M, Egawa S, Matsuda C, Onoyama Y, Morita K, Kakehi M, Sugahara T (1986) Multi-institutional studies on hyperthermia using an 8-MHz radiofrequency capacitive heating device (Thermotron RF-8) in combination with radiation for cancer therapy. Cancer 58(8):1589–1595
3. Baba H, Clifton Stephens L, Strebel FR, Siddik ZH, Newman RA, Ohno S, Bull JMC (1991) Protective Effect of ICRF-187 against normal tissue injury induced by Adriamycin in combination with whole body hyperthermia. Cancer Res 51(13):3568–3577
4. Ikeda NHO, Kameda H, Ito H, Matsuda T (1994) Experimental study on thermal damage to dog normal brain. Int J Hyperth 10(4):553–561
5. Lin JCWY (1987) Interstitial microwave antennas for thermal therapy. Int J Hyperth 3(1):37–47
6. Stauffer PR, Cetas TC, Fletcher AM, Deyoung DW, Dewhirst MW, Oleson JR, Roemer RB (1984) Observations on the use of ferromagnetic implants for inducing hyperthermia. Biomed Eng, IEEE Trans 31(1):76–90
7. Barry JW, Bookstein JJ, Alksne JF (1981) Ferromagnetic embolization. Experimental evaluation. Radiology 138(2):341–349
8. Rosensweig RE (2002) Heating magnetic fluid with alternating magnetic field. J Magn Magn Mater 252:370–374
9. Reimer P, Balzer T (2003) Ferucarbotran (Resovist): a new clinically approved RES-specific contrast agent for contrast-enhanced MRI of the liver: properties, clinical development, and applications. Eur Radiol 13(6):1266–1276
10. Hamm BST, Taupitz M, Maibauer R, Speidel A, Huppertz A, Frenzel T, Lawaczeck R, Wolf KJ, Lange L (1994) Contrast-enhanced MR imaging of liver and spleen: first experience in humans with a new superparamagnetic iron oxide. J Magn Reson Imaging 4(5):659–668

11. Takamatsu S, Matsui O, Gabata T, Kobayashi S, Okuda M, Ougi T, Ikehata Y, Nagano I, Nagae H (2008) Selective induction hyperthermia following transcatheter arterial embolization with a mixture of nano-sized magnetic particles (ferucarbotran) and embolic materials: feasibility study in rabbits. Radiat Med 26(4):179–187
12. Murase K, Oonoki J, Takata H, Song R, Angraini A, Ausanai P, Matsushita T (2011) Simulation and experimental studies on magnetic hyperthermia with use of superparamagnetic iron oxide nanoparticles. Radiol Phys Technol 4(2):194–202
13. Fram RJ (1992) Cisplatin and platinum analogues: recent advances. Curr Opin Oncol 4(6):1073–1079
14. Arany I, Safirstein RL (2003) Cisplatin nephrotoxicity. Semin Nephrol 23(5):460–464
15. Meyer KBMN (1994) Cisplatin nephrotoxicity. Min Electrolyte Metab 20(4):201–213
16. Pabla N, Dong Z (2008) Cisplatin nephrotoxicity: mechanisms and renoprotective strategies. Kidney Int 73(9):994–1007
17. Los G, Van Vugt MJH, Den Engelse L, Pinedo HM (1993) Effects of temperature on the interaction of cisplatin and carboplatin with cellular DNA. Biochem Pharmacol 46(7):1229–1237
18. Los G, van Vugt MJ, Pinedo HM (1994) Response of peritoneal solid tumours after intraperitoneal chemohyperthermia treatment with cisplatin or carboplatin. Br J Cancer 69(2):235–241
19. Barlogie B, Corry PM, Drewinko B (1980) In vitro thermochemotherapy of human colon cancer cells with *cis*-dichlorodiammineplatinum(II) and mitomycin C. Cancer Res 40(4):1165–1168
20. Cohen JD, Robins HI (1987) Hyperthermic enhancement of *cis*-Diammine-1,1-cyclobutane dicarboxylate platinum(II) cytotoxicity in human leukemia cells in vitro. Cancer Res 47(16): 4335–4337
21. Los GSP, Wondergem J, Mutsaers PH, Havemen J, ten Bokkel Huinink D, Smals O, Gonzalez-Gonzalez D, McVie JG (1991) Optimisation of intraperitoneal cisplatin therapy with regional hyperthermia in rats. Eur J Cancer 27(4):472–477
22. Wang X, Chen Y, Huang C, Wang X, Zhao L, Zhang X, Tang J (2013) Contribution of a 300 kHz alternating magnetic field on magnetic hyperthermia treatment of HepG2 cells. Bioelectromagnetics 34(2):95–103
23. Zhao QLW, Cheng R, Mao L, Arnold RD, Howerth EW, Chen ZG, Platt S (2012) Magnetic nanoparticle-based hyperthermia for head and neck cancer in mouse models. Theranostics 2(1):113–121
24. Atsumi T, Jeyadevan B, Sato Y, Tohji K (2007) Heating efficiency of magnetite particles exposed to AC magnetic field. J Magn Magn Mater 310(2):2841–2843
25. Hayashi KNM, Sakamoto W, Yogo T, Miki H, Ozaki S, Abe M, Matsumoto T, Ishimura K (2013) Superparamagnetic nanoparticle clusters for cancer theranostics combining magnetic resonance imaging and hyperthermia treatment. Theranostics 3(6):366–376
26. Nakao KOY, Akao Y, Ito Y, Marukawa O, Tachibana S, Kawakami M, Sasaki S (2000) The synergistic effects of hyperthermia and anticancer drugs on induction of apoptosis. Med Electron Microsc 33(1):44–50
27. Shao Y, Aplin AE (2010) Akt3-mediated resistance to apoptosis in B-RAF–targeted melanoma cells. Cancer Res 70(16): 6670–6681
28. Lee JT, Li L, Brafford PA, van den Eijnden M, Halloran MB, Sproesser K, Haass NK, Smalley KSM, Tsai J, Bollag G et al (2010) PLX4032, a potent inhibitor of the B-Raf V600E oncogene, selectively inhibits V600E-positive melanomas. Pigment Cell Melanoma Res 23(6):820–827
29. Al-Bahlani S, Fraser M, Wong AYC, Sayan BS, Bergeron R, Melino G, Tsang BK (2011) P73 regulates cisplatin-induced apoptosis in ovarian cancer cells via a calcium/calpain-dependent mechanism. Oncogene 30(41):4219–4230
30. Kopp AF, Laniado M, Dammann F, Stern W, Grönewäller E, Balzer T, Schimpfky C, Claussen CD (1997) MR imaging of the liver with Resovist: safety, efficacy, and pharmacodynamic properties. Radiology 204(3):749–756
31. Kusumoto TYM, Baba H, Takahashi I, Kusumoto H, Ohno S, Sugimachi K (1993) Sequence dependence of the hyperthermic potentiation of carboplatin-induced cytotoxicity and intracellular platinum accumulation in HeLa cells. Br J Cancer 68(2):259–263
32. Ito A, Honda H, Kobayashi T (2006) Cancer immunotherapy based on intracellular hyperthermia using magnetite nanoparticles: a novel concept of "heat-controlled necrosis" with heat shock protein expression. Cancer Immunol Immunother 55(3): 320–328
33. Mitsudo K, Koizumi T, Iida M, Iwai T, Oguri S, Yamamoto N, Itoh Y, Kioi M, Hirota M, Tohnai I (2012) Thermochemoradiation therapy using superselective intra-arterial infusion via superficial temporal and occipital arteries for oral cancer with N3 cervical lymph node metastases. Int J Radiat Oncol Biol Phys 83(5):639–645
34. Fukumura H, Sato M, Kezuka K, Sato I, Feng X, Okumura S, Fujita T, Yokoyama U, Eguchi H, Ishikawa Y et al (2012) Effect of ascorbic acid on reactive oxygen species production in chemotherapy and hyperthermia in prostate cancer cells. J Physiol Sci 62(3):251–257
35. Florea A-M, Büsselberg D (2011) Cisplatin as an anti-tumor drug: cellular mechanisms of activity, drug resistance and induced side effects. Cancers 3(1):1351–1371
36. Kim H-J, Lee J-H, Kim S-J, Oh GS, Moon H-D, Kwon K-B, Park C, Park BH, Lee H-K, Chung S-Y et al (2010) Roles of NADPH oxidases in cisplatin-induced reactive oxygen species generation and ototoxicity. J Neurosci 30(11):3933–3946
37. Jäckel M, Köpf-Maier P (1991) Influence of cisplatin on cell-cycle progression in xenografted human head and neck carcinomas. Cancer Chemother Pharmacol 27(6):464–471
38. Pucci B, Kasten M, Giordano A (2000) Cell cycle and apoptosis. Neoplasia 2(4):291–299
39. Aeq B (2004) Links between apoptosis, proliferation and the cell cycle. Br J Biomed Sci 61(2):99–102

Life Sciences 101 (2014) 43–48

Contents lists available at ScienceDirect

Life Sciences

journal homepage: www.elsevier.com/locate/lifescie

# Geranylgeranylacetone protects the heart via caveolae and caveolin-3

Yasuo M. Tsutsumi [a,*], Rie Tsutsumi [b], Yousuke T. Horikawa [a], Yoko Sakai [a], Eisuke Hamaguchi [a], Yoshihiro Ishikawa [c], Utako Yokoyama [c], Asuka Kasai [a], Noriko Kambe [a], Katsuya Tanaka [a]

[a] Department of Anesthesiology, University of Tokushima, Tokushima, Japan
[b] Department of Nutrition, University of Tokushima, Tokushima, Japan
[c] Cardiovascular Research Institute, Yokohama City University, Yokohama, Japan

ARTICLE INFO

*Article history:*
Received 5 November 2013
Accepted 12 February 2014
Available online 26 February 2014

*Keywords:*
Geranylgeranylacetone
Caveolin
Caveolae
Cardiac protection
Heat shock protein

ABSTRACT

*Aims:* Geranylgeranylacetone (GGA) is commonly utilized to protect the gastric mucosa in peptic ulcer disease. Recently GGA has been shown to protect the myocardium from ischemia/reperfusion by activating heat shock proteins. However, the exact mechanism as to how GGA activates these protective proteins is unknown. Caveolae and caveolin-3 (Cav-3) have been implicated in ischemia, anesthetic, and opioid induced cardiac protection. Given the lipophilic nature of GGA it is our hypothesis that GGA induced cardiac protection requires caveolae and Cav-3.

*Main methods:* We used an in vivo mouse model of ischemia–reperfusion injury and performed biochemical assays in excised hearts.

*Key findings:* GGA treated control mice revealed increased caveolae formation and caveolin-3 in buoyant fractions, mediating heat shock protein 70 activation. Furthermore, control mice treated with GGA were protected against ischemia/reperfusion injury whereas Cav-3 knockout (Cav-3 KO) mice were not. Troponin levels confirmed myocardial damage. Finally, Cav-3 KO mice treated with GGA were not protected against mitochondrial swelling whereas control mice had significant protection.

*Significance:* This study showed that caveolae and caveolin-3 are essential in facilitating GGA induced cardiac protection by optimizing spatial and temporal signaling to the mitochondria.



## Introduction

Geranylgeranylacetone (GGA), an acyclic polyisoprenoid, is commonly used as an oral anti-ulcer medication in Asia. This compound has been shown to be effective in protecting the gastric mucosa against insults without affecting gastric acid secretion (Fujimoto et al., 1982; Murakami et al., 1981). Oral GGA has been demonstrated to have protective effects on myocardial ischemia/reperfusion injury within the rat heart (Ooie et al., 2001). Yamanaka et al. suggested that GGA-induced cardiac preconditioning exerted protective effects on myocardial ischemia/reperfusion injury by mediating the activation of protein kinase C and heat shock protein (HSP) (Yamanaka et al., 2003). Further investigations demonstrated that GGA also prevented cellular endothelial damage (Zhu et al., 2005), diminished apoptosis and preserved mitochondrial respiratory function (Shinohara et al., 2007).

Structural scaffolding domains commonly organize signal transduction molecules and receptors. Caveolae are small membrane invaginations of the plasma membrane that are enriched in sphingolipids, cholesterol, and lipid rafts (Lisanti et al., 1994; Palade, 1953; Patel et al., 2008). Caveolins are the structural proteins of caveolae and are present in three isoforms, caveolin (Cav)-1, -2, and -3 (Lisanti et al., 1994; Patel et al., 2008). Additionally, many signaling molecules are known to localize in caveolae and interact with the scaffolding domain of caveolin. We have recently shown that both caveolae and Cav-3 were essential for ischemic (Horikawa et al., 2008; Tsutsumi et al., 2008), anesthetic (Horikawa et al., 2008), and opioid (Tsutsumi et al., 2010b) induced cardiac protection. It is our hypothesis that caveolin-3 and caveolae are also essential in GGA induced cardiac protection.

## Materials and methods

### Animals

All animals were treated in compliance with the Guidelines for Proper Conduct of Animal Experiment and Related Activities (Ministry of Education, Culture, Sports, Science and Technology of Japan) and the Guideline for Care and Use of Lab Animals at the University of

* Corresponding author at: Department of Anesthesiology, University of Tokushima, 3-18-15 Kuramoto, Tokushima 770-8503, Japan. Tel.: +81 88 633 7181; fax: +81 88 633 7182.
*E-mail address:* tsutsumi@tokushima-u.ac.jp (Y.M. Tsutsumi).

http://dx.doi.org/10.1016/j.lfs.2014.02.019
0024-3205/

Tokushima. Animal use protocols were approved by the Animal Care and Use Committee, the University of Tokushima. Male C57BL/6 mice (8–10 weeks old, 21–26 g body weight) were purchased from Japan SLC and Cav-3 knockout (Cav-3 KO) mice were created as reported previously (Hagiwara et al., 2000). Animals were randomly assigned into treatment groups by an independent observer. The animals were kept on a 12 hour light–dark cycle in a temperature-controlled room. GGA was provided by Eisai Co., Tokyo, Japan and was given by gavage at a dose of 200 mg/kg (dissolved with 0.4% lecithin in deionized water). Mice in the control group were given the same dose of vehicle.

*Electron microscopy*

Wild-type mice were given GGA or vehicle by oral gavage. Twenty four hours later, whole hearts were fixed with 2.5% glutaraldehyde in 0.1 M cacodylate buffer for 2 h at room temperature, post-fixed in 1% $OsO_4$ in 0.1 M cacodylate buffer (1 h), and uranyl acetate, dehydrated in a graded series of ethanol solutions, and embedded in epon epoxy resin. Sections were cut with a Reichert Ultracut E Ultramicrotome (Leica Microsystems, Wetzlar, Germany) and observed with an electron microscope (Hitachi H7650, Hitachi Co., Tokyo, Japan). Random sections were taken by an electron microscopy technician blinded to the treatments.

*Sucrose density membrane fractionation*

We performed whole left ventricle sucrose density membrane fractions as reported previously (Tsutsumi et al., 2008). Fraction samples 4–12 were used in immunoblot analyses. We defined fractions 4–6 as lipid rich–buoyant membrane fractions enriched in caveolae and proteins associated with caveolae. Fractions 9–12 were defined as non-buoyant fractions.

*Immunoblot analysis*

Proteins in whole left ventricle or membrane fractions were separated by SDS-PAGE 10% polyacrylamide precast gels (Bio-Rad Laboratories) and transferred to a polyvinylidene difluoride membrane by electroelution. Membranes were blocked in PBS containing 2.0% nonfat dry milk and incubated with primary antibody overnight at 4 °C. Bound primary antibodies were visualized using secondary antibodies conjugated with horseradish peroxidase from Santa Cruz Biotechnology (Santa Cruz) and ECL reagent from Amersham Pharmacia. All displayed bands migrated at the appropriate size, as determined by comparison to molecular weight standards (Santa Cruz Biotechnology).

*Immunoprecipitation*

Immunoprecipitation was performed using Protein A Sepharose CL-4B (GE Healthcare) as described previously (Hirose et al., 2011). Buoyant fraction samples were incubated with primary antibody for 3 h at 4 °C, immunoprecipitated overnight with protein-agarose at 4 °C, and then centrifuged for 5 min at 13,000 *g*. Protein-agarose pellets were washed 3 times. Wash buffer was removed and sample buffer was added, and then boiled for 5 min at 95 °C for immunoblotting.

*Ischemia–reperfusion protocol and experimental groups*

Cav-3 KO and control mice were randomly assigned to receive GGA or vehicle 24 h before ischemic injury. Mice were anesthetized with pentobarbital sodium (80 mg/kg i.p.) and mechanically ventilated by using a pressure-controlled ventilator (TOPO Ventilator, Kent Scientific) as described before (Tsutsumi et al., 2006, 2007). Core temperature was maintained with a heating pad and ECG leads were placed to record heart rate. The hemodynamic effects were measured through the right carotid artery cannulation with a 1.4F Mikro-tip pressure transducer (Model SPR-671, Millar Instruments), which was connected to an amplifier (Model TC-510, Millar Instruments) for determination of heart rate, arterial blood pressure, and rate pressure product.

Lethal ischemia was produced by occluding the left coronary artery with a 7–0 silk suture placed with a tapered BV-1 needle (Ethicon) for 30 min. After 30 min of occlusion, the ligature was released and the heart was reperfused for 2 h. After reperfusion, mice were heparinized, and the coronary artery was again occluded. The area at risk (AAR) was determined by staining with 1% Evans blue (1.0 mL, Sigma). The heart was immediately excised and cut into 1.0-mm slices (McIlwain tissue chopper; Brinkmann Instruments). Each slice of left ventricle (LV) was then counterstained with 2,3,5,-triphenyltetrazolium chloride (Sigma). After overnight storage in 10% formaldehyde, slices were weighed and visualized under a microscope (SZ61-TR, Olympus) equipped with a charge coupled device camera (DXM 1200F, Nikon). The images were analyzed (Image-Pro Plus, Media Cybernetics), and area at risk (AAR) and infarct size (IS) were determined by planimetry as previously described (Tsutsumi et al., 2008; Horikawa et al., 2008). Cardiac troponin I (cTnI) levels in the serum were measured using a High Sensitivity Mouse Cardiac Troponin-I ELISA Kit (Life Diagnostics) as described before (Tsutsumi et al., 2010a).

*Mitochondrial isolation and swelling assay*

Mice were anesthetized and hearts were harvested, immediately rinsed with PBS, and placed in homogenizer containing 4 mL sucrose buffer A (300 mM sucrose, 10 mM Tris–HCl, 2 mM EGTA and 5 mg/mL BSA, pH 7.4) on ice. Hearts were homogenized using 10 strokes and homogenate centrifuged at 2000 ×*g* for 2 min at 4 °C to remove cell debris. The supernatant was further centrifuged at 10,000 ×*g* for 30 min at 4 °C to sediment impure mitochondria. Mitochondrial pellet was purified and washed as described previously (Fridolfsson et al., 2012). 200 μL of mitochondria in sucrose buffer B (300 mM sucrose, 10 mM Tris–HCl, pH 7.4) was loaded on to 96-well plate and challenged with 100 μM $CaCl_2$ (2 mg/mL protein concentration). Absorbance was measured every 2 s for 600 measurements at 520 nm using a VarioSkan Flash spectrophotometer (Thermo Scientific). 250 nM cyclosporine A (Sigma) pretreatment of mitochondria was used to inhibit $CaCl_2$ induced mitochondrial swelling to confirm the mitochondrial permeability transition pore (mPTP) dependence of calcium-induced swelling.

*Statistical analysis*

Determination of all data was performed blinded to experimental groups for the observers. Data were analyzed using Prism 6.0 (GraphPad Software, Inc.). Statistical analyses for Western blot studies were performed using Student's *t*-tests. When one-way ANOVA was needed, the Bonferroni post-hoc test was used. All data are expressed as mean ± SD. Statistical significance was defined as $P < 0.05$

## Results

The effect of GGA on cardiac membrane caveolae was assessed by pre-treating mice with and without GGA and performing electron microscopy analysis. Representative electron microscopy images show that pretreatment of GGA increased membrane caveolae compared to vehicle treated control animals (Fig. 1). However, Cav-3 KO mice had significantly decreased caveolae with no significant change after GGA treatment (data not shown). To verify these findings, hearts from GGA and vehicle control animals were fractionated on a discontinuous sucrose gradient and analyzed for protein content. GGA increased both Cav-3 protein expression and HSP 70 expression in buoyant fractions 4–6, which are associated with caveolae (Fig. 2A and 2B). Additionally, immunoprecipitation experiments showed that GGA treated mice resulted in HSP 70 associated with Cav-3 in buoyant fractions (Fig. 2C), suggesting that Cav-3 is essential for HSP 70 localization and activation.

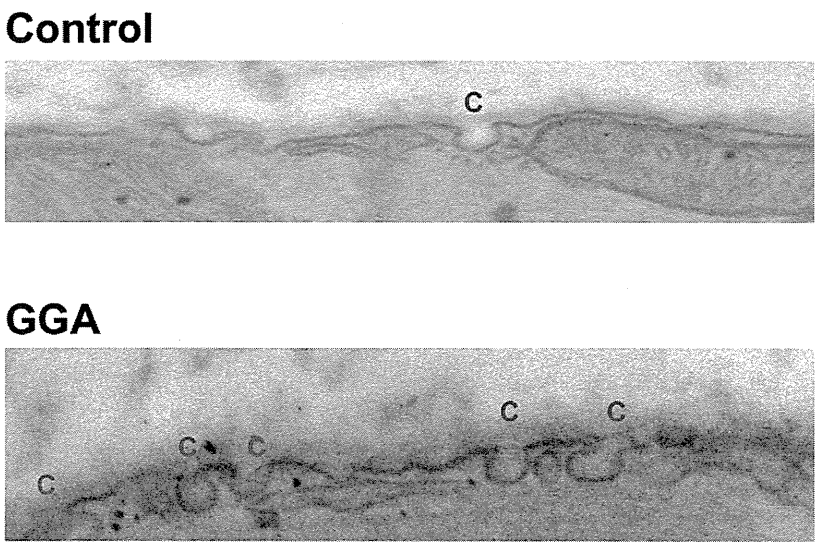


**Fig. 1.** Geranylgeranylacetone (GGA) increases myocardial caveolae. Electron microscopy of control and GGA treated mouse myocardium revealed a significant increase in caveolae (red C) at the sarcolemmal surface in GGA treated mice.

We found no significant differences between wild-type and Cav-3 KO mice in heart rate, blood pressure, or rate pressure product with and without GGA administration at the baseline period (Table 1). The area at risk was calculated as a percentage of the left ventricle mass and was similar between groups (Fig. 3A). Twenty-four hours after GGA administration, a significant reduction in myocardial ischemia/reperfusion injury was observed compared with vehicle control in the wild-type mice (29.0 ± 3.7% [n = 8] vs. 44.1 ± 9.3% [n = 10],

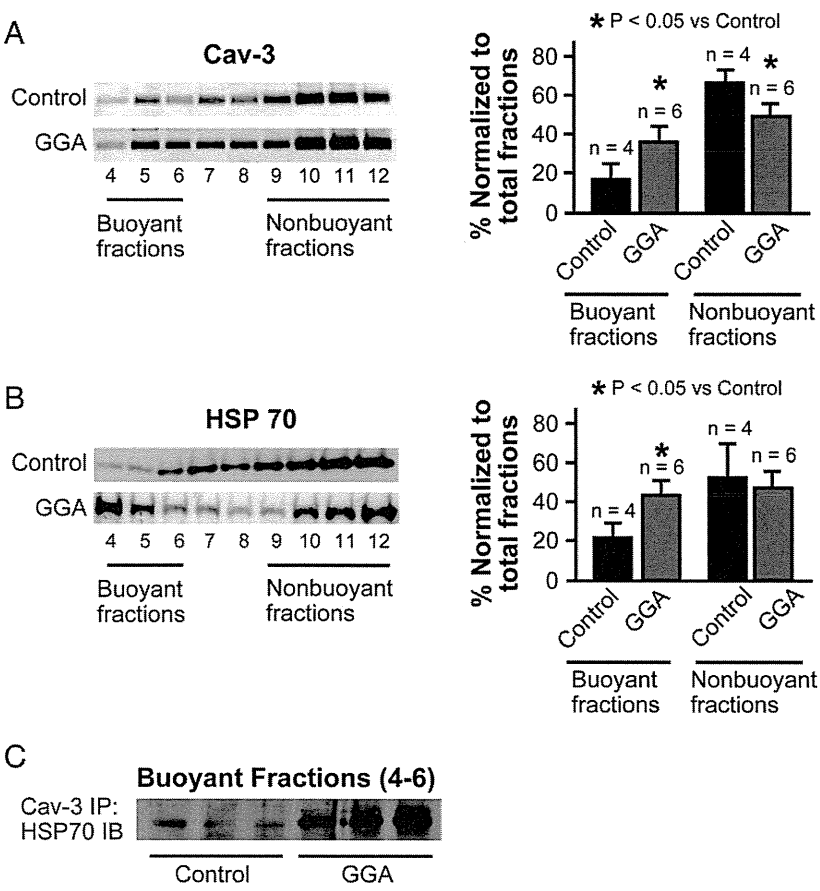


**Fig. 2.** Lysed and fractionated hearts on a sucrose density gradient. Fractions 4–6 were considered buoyant and 9–12 non-buoyant fractions. *P < 0.05 treated group versus control. A) and B) Fractions were collected and probed for both caveolin-3 (Cav-3) and heat shock protein 70 (HSP 70). Significant buoyant fraction localization of Cav-3 and HSP 70 was observed in geranylgeranylacetone (GGA) treated groups. C) The resulting lysates were immunoprecipitated (IP) with Cav-3 antibody and immunoblotted (IB) for HSP 70; n = 3 animals per group. There was an increased association of Cav-3 with HSP 70 after GGA administration.

**Table 1**
Hemodynamics parameters at baseline period.

| | Control | GGA | Cav-3 KO | GGA + Cav-3 KO |
|---|---|---|---|---|
| Heart rate (/min) | 421 ± 33 | 437 ± 21 | 413 ± 35 | 426 ± 37 |
| MAP (mm Hg) | 73 ± 6 | 69 ± 8 | 71 ± 4 | 70 ± 3 |
| RPP (beats·min$^{-1}$·mm Hg·10$^3$) | 30.5 ± 3.7 | 30.0 ± 3.3 | 29.4 ± 4.0 | 29.8 ± 2.3 |

MAP, mean arterial pressure; RPP, rate-pressure product. Data are expressed as mean ± SD.

respectively). However, in Cav-3 KO mice, this cardiac-protective effect of GGA was abolished (42.1 ± 5.2% [n = 8], Fig. 3B). Additionally, we confirmed these effects by measuring serum troponin I level, a marker of cardiac myocyte damage (Fig. 3C).

GGA reduces $Ca^{2+}$-induced swelling in isolated mouse heart mitochondria (Fig. 4). In wild-type mice, the addition of 100 μM $Ca^{2+}$ caused a significant decrease in absorbance, indicating mitochondrial swelling. $Ca^{2+}$ induced swelling was inhibited by cyclosporine A, a mPTP inhibitor, as reported previously (Tsutsumi et al., 2011). Under these conditions, GGA significantly attenuated $Ca^{2+}$ induced swelling compared with the control; however, these effects were abolished in Cav-3 KO mice.

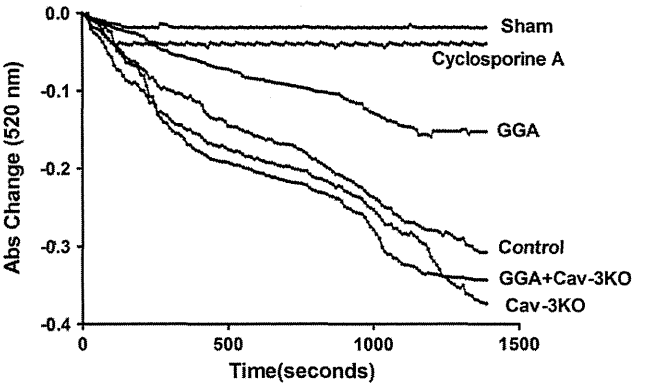


**Fig. 4.** Geranylgeranylacetone (GGA) inhibits mitochondrial swelling caused by ischemia-reperfusion injury. GGA treated mitochondria were isolated and revealed substantially less mitochondrial swelling compared to non-treated and Cav-3 KO mice with and without GGA when exposed to calcium chloride. Cyclosporine A was used as a control to inhibit $CaCl_2$ induced mitochondrial swelling to confirm the mitochondrial permeability transition pore (mPTP) dependence of calcium-induced swelling (n = 3).

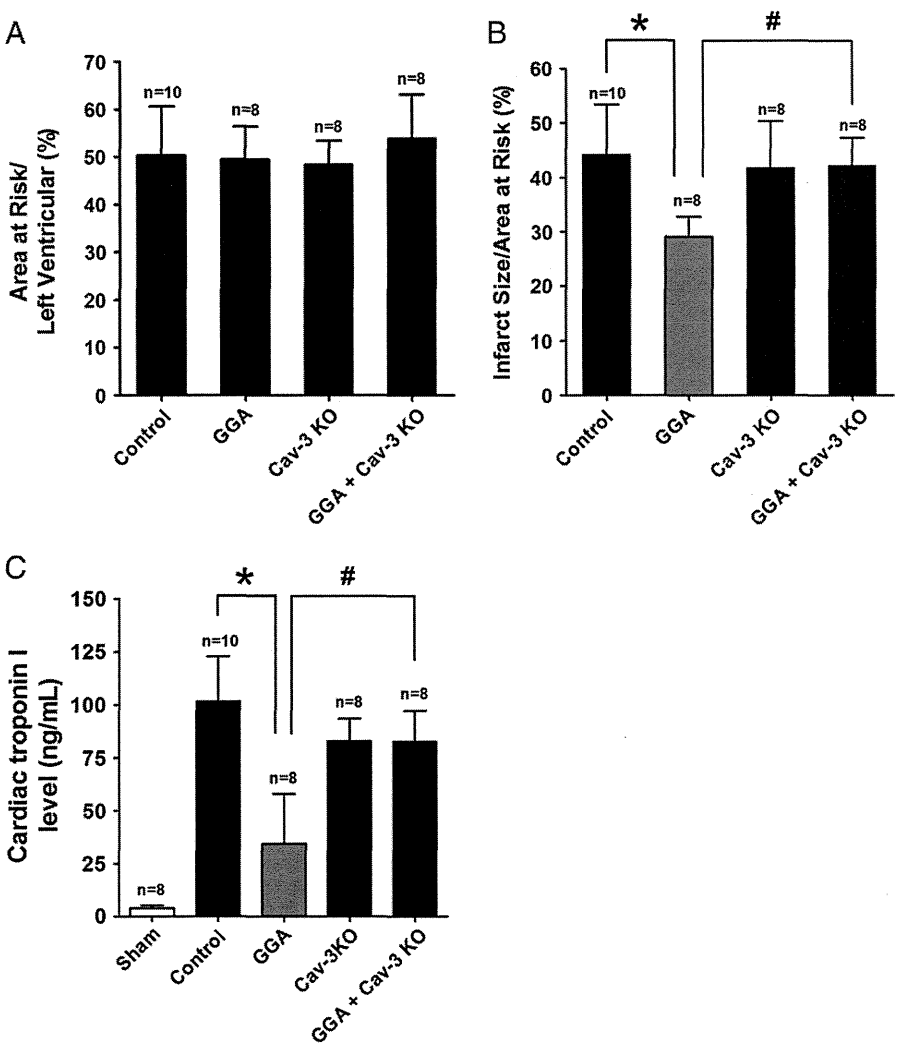


**Fig. 3.** Geranylgeranylacetone (GGA) protects the mouse myocardium from ischemic injury. A) Area at risk was calculated as a percentage of the left ventricle and revealed no significant differences between all groups. B) GGA was able to induce significant protection in control animals, although no protection was observed in Cav-3 KO mice. C) Cardiac troponin I, a marker of myocardial damage also revealed a significant decrease in GGA treated control mice, but no effect in Cav-3 KO mice. * $P < 0.05$; # $P < 0.05$.

## Discussion

GGA, an anti-ulcer medication has been shown to have cardio-protective effects and modulate heat shock proteins, however the exact mechanisms on how this oral medication is able to enter the myocardial cell is unknown. We show that caveolae and Cav-3 are essential for GGA uptake and cardiac protection, by mediating the activation of HSP 70. Furthermore, these effects are not only mediated by caveolae and caveolins, but also directly affect mitochondrial function. These data suggest that GGA utilizes caveolae and caveolins in order to navigate the complex cell structure and facilitate protective signaling via mitochondria.

Caveolae are cholesterol and sphingolipid enriched invaginations of the plasma membrane that play a role in physiological functions and vital to cardio-protective mechanisms. In some cases, caveolae and caveolins regulate receptor stability, myocardial hypertrophy (Horikawa et al., 2011), signaling (Lisanti et al., 1994; Ostrom et al., 2001, 2002; Patel et al., 2007; Steinberg and Brunton, 2001), calcium homeostasis (Fujimoto, 1993), and endocytosis (Anderson, 1993). Recently, a decreased number of myocardial caveolae was described in Cav-3 KO mice although Cav-1 levels remained stable (Hagiwara et al., 2000; Horikawa et al., 2008; Tsutsumi et al., 2010b). Furthermore, these mice lose the ability to undergo preconditioning-like cardiac protection from ischemia/reperfusion injury (Horikawa et al., 2008). These results implicate a role for Cav-3 and the presence of caveolae in cardiac protection from ischemia/reperfusion injury. The current data show that GGA similarly requires Cav-3 and caveolae. These effects are likely due to the ability of Cav-3 and caveolae to be able to regulate mitochondrial pore activity and mediate mitochondrial mediated cell death. Furthermore, recent investigations have revealed that caveolae and caveolins can directly interact with mitochondria and regulate mitochondrial function, suggesting a potential regulatory role in surface and inter-organelle signaling (Fridolfsson et al., 2012).

In the present study, we show that the administration of GGA led to a significant increase in Cav-3 protein expression within the buoyant fraction, and that HSP 70 directly localized and interacted with Cav-3. Many previous studies using GGA have focused on HSP 70 induction (Hirakawa et al., 1996; Sakabe et al., 2008) and have suggested that GGA protects the myocardium by activating heat shock proteins especially HSP 72 (Kitahata et al., 2008; Ooie et al., 2005; Ooie et al., 2001; Yamanaka et al., 2003). Although there has been little evidence regarding the relationship between caveolae, caveolins and heat shock proteins within the heart, other organ systems including skin and cancer have investigated this relationship. In skin models, HSP have been shown to localize into caveolae, which then can regulate intracellular HSP expression (Black et al., 2011). Furthermore, in tumor cells, Cav-1 has been shown to have direct effects on HSP expression (Ciocca et al., 2012). Perhaps, in regard to GGA, caveolae are spatial hubs that localize GGA and HSP, together regulating temporal relations and activation. Given the multifaceted nature of caveolae and caveolins, multiple survival pathways are being activated simultaneously.

Glucose transporter 4 receptor (Glut4) has also been implicated in delayed preconditioning of the myocardium. Interestingly, Cav-3 KO mice are unable to be protected via isoflurane, due to its inability to translocate Glut 4, although this is preserved in Cav-1 KO, making this a Cav-3 specific phenomenon (Tsutsumi et al., 2010b). Perhaps GGA may also have effects on Glut4 translocation and expression.

There are several limitations in the present study. First, we evaluated the effects of Cav-3 and HSP 70 in experiments that investigated ischemia/reperfusion injury. GGA induces a broad class of the protective proteins, including various families of HSPs (Brundel et al., 2006a, 2006b), protein kinase C (Yamanaka et al., 2003), and nitric oxide (Yamamoto et al., 2005). Second, the dose and time period used for cardiac protection in mice are unknown. Previous studies have all been in rats, where a single oral dose of 200 mg/kg GGA induced HSP and cardiac protection against ischemia/reperfusion (Ooie et al., 2005, 2001; Shinohara et al., 2007; Yamanaka et al., 2003). The same concentration and dose were applied in this study.

Taken together these data demonstrate that GGA had delayed cardio-protective effects that are dependent on caveolae and Cav-3. We show that caveolae and Cav-3 are the vital conduits between HSP-70 activation and subsequent mitochondrial respiration suggesting an important role for this structural protein. Furthermore, these data suggest that GGA may be a unique way to clinically increase caveolae and caveolin-3 expression, which have both shown to have significant cardioprotective effects against ischemic injury and detrimental remodeling.

### Conflict of interest statement

The authors declare that there are no conflicts of interest.

## Acknowledgments

Supported by JSPS KAKENHI Numbers 23592994, 24592300, 25462404, and 25462405 from Japan Society for the Promotion of Science, Tokyo.

## References

Anderson RG. Potocytosis of small molecules and ions by caveolae. Trends Cell Biol 1993; 3:69–72.
Black AT, Hayden PJ, Casillas RP, Heck DE, Gerecke DR, Sinko PJ, et al. Regulation of Hsp27 and Hsp70 expression in human and mouse skin construct models by caveolae following exposure to the model sulfur mustard vesicant, 2-chloroethyl ethyl sulfide. Toxicol Appl Pharmacol 2011;253:112–20.
Brundel BJ, Henning RH, Ke L, van Gelder IC, Crijns HJ, Kampinga HH. Heat shock protein upregulation protects against pacing-induced myolysis in HL-1 atrial myocytes and in human atrial fibrillation. J Mol Cell Cardiol 2006a;41:555–62.
Brundel BJ, Shiroshita-Takeshita A, Qi X, Yeh YH, Chartier D, van Gelder IC, et al. Induction of heat shock response protects the heart against atrial fibrillation. Circ Res 2006b;99: 1394–402.
Ciocca DR, Cuello-Carrion FD, Natoli AL, Restall C, Anderson RL. Absence of caveolin-1 alters heat shock protein expression in spontaneous mammary tumors driven by Her-2/neu expression. Histochem Cell Biol 2012;137:187–94.
Fridolfsson HN, Kawaraguchi Y, Ali SS, Panneerselvam M, Niesman IR, Finley JC, et al. Mitochondria-localized caveolin in adaptation to cellular stress and injury. FASEB J 2012;26:4637–49.
Fujimoto T. Calcium pump of the plasma membrane is localized in caveolae. J Cell Biol 1993;120:1147–57.
Fujimoto M, Yamanaka T, Bessho M, Igarashi T. Effects of geranylgeranylacetone on gastrointestinal secretion in rats. Eur J Pharmacol 1982;77:113–8.
Hagiwara Y, Sasaoka T, Araishi K, Imamura M, Yorifuji H, Nonaka I, et al. Caveolin-3 deficiency causes muscle degeneration in mice. Hum Mol Genet 2000;9:3047–54.
Hirakawa T, Rokutan K, Nikawa T, Kishi K. Geranylgeranylacetone induces heat shock proteins in cultured guinea pig gastric mucosal cells and rat gastric mucosa. Gastroenterology 1996;111:345–57.
Hirose K, Tsutsumi YM, Tsutsumi R, Shono M, Katayama E, Kinoshita M, et al. Role of the O-linked beta-N-acetylglucosamine in the cardioprotection induced by isoflurane. Anesthesiology 2011;115:955–62.
Horikawa YT, Patel HH, Tsutsumi YM, Jennings MM, Kidd MW, Hagiwara Y, et al. Caveolin-3 expression and caveolae are required for isoflurane-induced cardiac protection from hypoxia and ischemia/reperfusion injury. J Mol Cell Cardiol 2008;44: 123–30.
Horikawa YT, Panneerselvam M, Kawaraguchi Y, Tsutsumi YM, Ali SS, Balijepalli RC, et al. Cardiac-specific overexpression of caveolin-3 attenuates cardiac hypertrophy and increases natriuretic peptide expression and signaling. J Am Coll Cardiol 2011;57: 2273–83.
Kitahata H, Nozaki J, Kawahito S, Tomino T, Oshita S. Low-dose sevoflurane inhalation enhances late cardioprotection from the anti-ulcer drug geranylgeranylacetone. Anesth Analg 2008;107:755–61.
Lisanti MP, Scherer PE, Tang Z, Sargiacomo M. Caveolae, caveolin and caveolin-rich membrane domains: a signalling hypothesis. Trends Cell Biol 1994;4:231–5.
Murakami M, Oketani K, Fujisaki H, Wakabayashi T, Ohgo T. Antiulcer effect of geranylgeranylacetone, a new acyclic polyisoprenoid on experimentally induced gastric and duodenal ulcers in rats. Arzneimittelforschung 1981;31:799–804.
Ooie T, Takahashi N, Saikawa T, Nawata T, Arikawa M, Yamanaka K, et al. Single oral dose of geranylgeranylacetone induces heat-shock protein 72 and renders protection against ischemia/reperfusion injury in rat heart. Circulation 2001;104: 1837–43.
Ooie T, Kajimoto M, Takahashi N, Shinohara T, Taniguchi Y, Kouno H, et al. Effects of insulin resistance on geranylgeranylacetone-induced expression of heat shock protein 72 and cardioprotection in high-fat diet rats. Life Sci 2005;77:869–81.
Ostrom RS, Gregorian C, Drenan RM, Xiang Y, Regan JW, Insel PA. Receptor number and caveolar co-localization determine receptor coupling efficiency to adenylyl cyclase. J Biol Chem 2001;276:42063–9.

Ostrom RS, Liu X, Head BP, Gregorian C, Seasholtz TM, Insel PA. Localization of adenylyl cyclase isoforms and G protein-coupled receptors in vascular smooth muscle cells: expression in caveolin-rich and noncaveolin domains. Mol Pharmacol 2002;62: 983–92.

Palade G. Fine structure of blood capillaries. J Appl Phys 1953;24:1424–36.

Patel HH, Tsutsumi YM, Head BP, Niesman IR, Jennings M, Horikawa Y, et al. Mechanisms of cardiac protection from ischemia/reperfusion injury: a role for caveolae and caveolin-1. FASEB J 2007;21:1565–74.

Patel HH, Murray F, Insel PA. Caveolae as organizers of pharmacologically relevant signal transduction molecules. Annu Rev Pharmacol Toxicol 2008;48: 359–91.

Sakabe M, Shiroshita-Takeshita A, Maguy A, Brundel BJ, Fujiki A, Inoue H, et al. Effects of a heat shock protein inducer on the atrial fibrillation substrate caused by acute atrial ischaemia. Cardiovasc Res 2008;78:63–70.

Shinohara T, Takahashi N, Kohno H, Yamanaka K, Ooie T, Wakisaka O, et al. Mitochondria are targets for geranylgeranylacetone-induced cardioprotection against ischemia–reperfusion in the rat heart. Am J Physiol Heart Circ Physiol 2007;293: H1892–9.

Steinberg SF, Brunton LL. Compartmentation of G protein-coupled signaling pathways in cardiac myocytes. Annu Rev Pharmacol Toxicol 2001;41:751–73.

Tsutsumi YM, Patel HH, Lai NC, Takahashi T, Head BP, Roth DM. Isoflurane produces sustained cardiac protection after ischemia–reperfusion injury in mice. Anesthesiology 2006;104:495–502.

Tsutsumi YM, Yokoyama T, Horikawa Y, Roth DM, Patel HH. Reactive oxygen species trigger ischemic and pharmacological postconditioning: in vivo and in vitro characterization. Life Sci 2007;81:1223–7.

Tsutsumi YM, Horikawa YT, Jennings MM, Kidd MW, Niesman IR, Yokoyama U, et al. Cardiac-specific overexpression of caveolin-3 induces endogenous cardiac protection by mimicking ischemic preconditioning. Circulation 2008;118:1979–88.

Tsutsumi YM, Kawaraguchi Y, Horikawa YT, Niesman IR, Kidd MW, Chin-Lee B, et al. Role of caveolin-3 and glucose transporter-4 in isoflurane-induced delayed cardiac protection. Anesthesiology 2010a;112:1136–45.

Tsutsumi YM, Kawaraguchi Y, Niesman IR, Patel HH, Roth DM. Opioid-induced preconditioning is dependent on caveolin-3 expression. Anesth Analg 2010b;111:1117–21.

Tsutsumi YM, Tsutsumi R, Mawatari K, Nakaya Y, Kinoshita M, Tanaka K, et al. Compound K, a metabolite of ginsenosides, induces cardiac protection mediated nitric oxide via Akt/PI3K pathway. Life Sci 2011;88:725–9.

Yamamoto K, Sarukawa M, Ito T, Aoki H, Ichida M, Shimada K. An anti-ulcer drug, geranylgeranylacetone, suppresses inducible nitric oxide synthase in cultured vascular smooth muscle cells. J Hypertens 2005;23:1847–53.

Yamanaka K, Takahashi N, Ooie T, Kaneda K, Yoshimatsu H, Saikawa T. Role of protein kinase C in geranylgeranylacetone-induced expression of heat-shock protein 72 and cardioprotection in the rat heart. J Mol Cell Cardiol 2003;35:785–94.

Zhu Z, Takahashi N, Ooie T, Shinohara T, Yamanaka K, Saikawa T. Oral administration of geranylgeranylacetone blunts the endothelial dysfunction induced by ischemia and reperfusion in the rat heart. J Cardiovasc Pharmacol 2005;45:555–62.

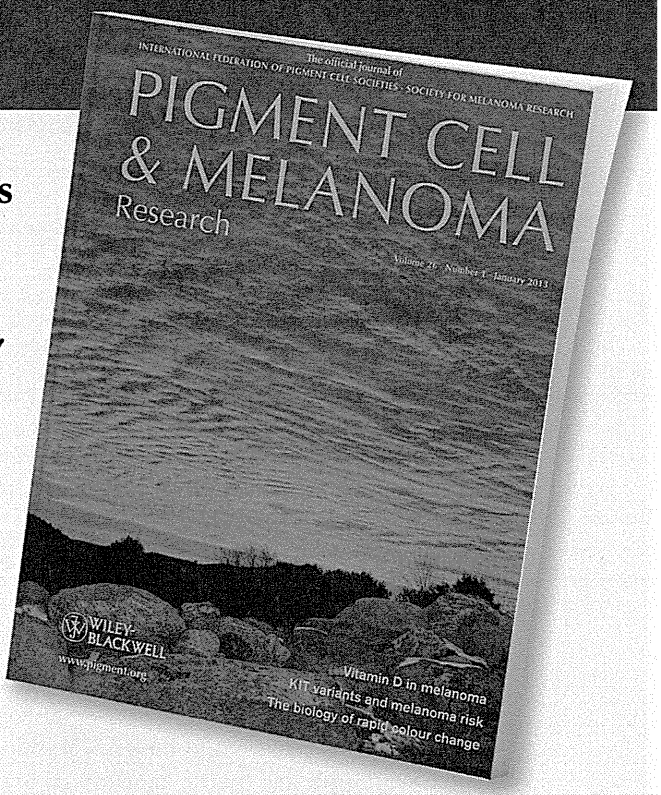


## Epac1 increases migration of endothelial cells and melanoma cells via FGF2-mediated paracrine signaling

**Erdene Baljinnyam, Masanari Umemura, Christine Chuang, Mariana S. De Lorenzo, Mizuka Iwatsubo, Suzie Chen, James S. Goydos, Yoshihiro Ishikawa, John M. Whitelock and Kousaku Iwatsubo**

**DOI: 10.1111/pcmr.12250**

# Epac1 increases migration of endothelial cells and melanoma cells via FGF2-mediated paracrine signaling

**Erdene Baljinnyam[1], Masanari Umemura[1,2], Christine Chuang[3], Mariana S. De Lorenzo[1], Mizuka Iwatsubo[1], Suzie Chen[4], James S. Goydos[5], Yoshihiro Ishikawa[1,2], John M. Whitelock[6] and Kousaku Iwatsubo[1,2]**

**1** Department of Cell Biology and Molecular Medicine, New Jersey Medical School-Rutgers, The State University of New Jersey, Newark, NJ, USA **2** Cardiovascular Research Institute, Yokohama City University Graduate School of Medicine, Yokohama, Japan **3** The Heart Research Institute, Newtown, NSW, Australia **4** Susan Lehman Cullman Laboratory for Cancer Research Ernest Mario School of Pharmacy, Rutgers, The State University of New Jersey, Piscataway, NJ, USA **5** The Cancer Institute of New Jersey, New Brunswick, NJ, USA **6** Graduate School of Biomedical Engineering, The University of New South Wales, Kensington, NSW, Australia

**CORRESPONDENCE** Kousaku Iwatsubo and Erdene Baljinnyam, e-mails: iwatsuko@njms.rutgers.edu; baljiner@njms.rutgers.edu

**KEYWORDS** Epac/heparan sulfate/human umbilical vein endothelial cells/cell–cell communication/FGF2/migration/angiogenesis/paracrine signaling

**PUBLICATION DATA** Received 5 April 2013, revised and accepted for publication 9 April 2014, published online 11 April 2014

doi: 10.1111/pcmr.12250

## Summary

**Fibroblast growth factor (FGF2) regulates endothelial and melanoma cell migration. The binding of FGF2 to its receptor requires N-sulfated heparan sulfate (HS) glycosamine. We have previously reported that Epac1, an exchange protein activated by cAMP, increases N-sulfation of HS in melanoma. Therefore, we examined whether Epac1 regulates FGF2-mediated cell–cell communication. Conditioned medium (CM) of melanoma cells with abundant expression of Epac1 increased migration of human umbilical endothelial cells (HUVEC) and melanoma cells with poor expression of Epac1. CM-induced increase in migration was inhibited by antagonizing FGF2, by the removal of HS and by the knockdown of Epac1. In addition, knockdown of Epac1 suppressed the binding of FGF2 to FGF receptor in HUVEC, and *in vivo* angiogenesis in melanoma. Furthermore, knockdown of Epac1 reduced N-sulfation of HS chains attached to perlecan, a major secreted type of HS proteoglycan that mediates the binding of FGF2 to FGF receptor. These data suggested that Epac1 in melanoma cells regulates melanoma progression via the HS–FGF2-mediated cell–cell communication.**

## Introduction

Despite recent advances in melanoma therapies utilizing inhibitors of the ERK-signaling pathway, prognosis of advanced melanoma is still poor. In addition, acquired resistance becomes a critical problem with those inhibitors (Little et al., 2012; Maurer et al., 2011). Therefore, the development of a novel therapeutic strategy is an urgent demand for this life-threatening disease. cAMP signaling controls a variety of cellular functions in cancer cells. Exchange protein activated by cAMP (Epac), a guanine nucleotide exchange factor, was found as an additional target of cAMP apart from the conventional one, that is, protein kinase A (De Rooij et al., 1998). Two isoforms of Epac, Epac1 and Epac2, mediate cAMP signaling by the activation of a small-molecular-weight G protein, Rap1 (Bos, 2006). In cancer cells, reports have demonstrated following functions of Epacs such as cell adhesion in human ovarian carcinoma Ovcar3 cells (Quilliam et al., 2002), apoptosis (Tiwari et al., 2004)

### Significance

There is an emerging need for elucidating the mechanism of cell–cell interaction in melanoma progression. Our study provides information regarding FGF2-related cell–cell interaction between melanoma/endothelial and melanoma/melanoma cells which is regulated by melanoma cells with the higher expression of Epac1.

and growth arrest (Grandoch et al., 2009a) in B lymphoma cells, formation of embryonic vasculogenic networks in melanoma cells (Lissitzky et al., 2009), and proliferation of prostate carcinoma cells (Grandoch et al., 2009b). We have previously reported that Epac1 is expressed in various melanoma cell lines (Baljinnyam et al., 2011) and plays a role in cell migration via modification of heparan sulfate (HS) glycosaminoglycan (HSPG) chains. The increased migration by Epac1-enhanced metastasis to the lungs in mice (Baljinnyam et al., 2009). Recently, we have also found that, in addition to this HS-related mechanism, a $Ca^{2+}$-dependent mechanism is also involved in Epac1-induced melanoma cell migration. Epac1 releases cytosolic $Ca^{2+}$ from the endoplasmic reticulum (ER) via the phospholipase C (PLC)/inositol triphosphate (IP3)/IP3 receptor pathway (Baljinnyam et al., 2010). These data suggested that Epac1 plays a critical role in melanoma cell migration via at least two independent mechanisms, that is, the HS-related and the $Ca^{2+}$-dependent mechanisms.

Fibroblast growth factor-2 (FGF2) is known to increase tumor growth and metastasis by the activation of migration of cancer and vascular endothelial cells (Hibino et al., 2005; Meier et al., 2003; Montesano et al., 1986; Moscatelli et al., 1986; Nugent et al., 2000; Ponta et al., 1998; Sola et al., 1997; Taylor et al., 1993). Binding of FGF2 to FGF receptor requires coordination with N-sulfated glucosamine (Faham et al., 1996; Kreuger et al., 1999; Maccarana et al., 1993; Schlessinger et al., 2000), a component of HS chain (Iozzo and San Antonio, 2001). In addition, perlecan, one of the HSPGs, attaches to FGF2 for its binding to FGF receptors (Knox et al., 2002; Sharma et al., 1998). We have previously reported that, in a human melanoma cell line, Epac1 increases NDST-1, which converts N-acetylated glucosamine into N-sulfated form (Baljinnyam et al., 2009). In addition, it was suggested that Epac1 overexpression increases N-sulfation of HS chain (Baljinnyam et al., 2009).These data led us to examine the hypothesis that Epac1 can control FGF2 signaling by modification of N-sulfation of HS, most probably on perlecan. Further, as secreted FGF2 can act in a paracrine fashion, it is possible that melanoma cells expressing Epac1 regulate migration of surrounding endothelial or other melanoma cells. In this study, we found that Epac1 in melanoma cells increases N-sulfation of secreted perlecan and activates migration of endothelial/melanoma cells by FGF2/HS-mediated cell-cell interaction. In addition, the Epac1 in melanoma cells activates angiogenesis *in vivo*, which may support the survival of other melanoma cells expressing lower amounts of Epac1. Therefore, in addition to our previous reports showing the role of Epac1 in melanoma cells, this study demonstrated that expression of Epac1 in melanoma cells plays a role in melanoma progression by controlling cell/cell communication with endothelial cells and other melanoma cells.

## Results

### Epac1 in melanoma cells increases migration of neighboring endothelial cells via cell/cell communication

It was suggested that Epac1-expressing melanoma cells can increase migration of neighboring endothelial cells via N-sulfation of HSPG, and subsequently, the activation of paracrine-acting FGF2 signaling. Therefore, we investigated whether melanoma cells with abundant Epac1 expression can increase migration of those with scarce Epac1 expression. According to our previous report (Baljinnyam et al., 2010, 2011), in this study, we have divided the cell lines into two groups: Epac1-rich cell lines, in which Epac1 expression is of the same or higher level than that in SK-Mel-2 (SK-Mel-2, SK-Mel-24, SK-Mel187, and C8161 cells). Epac1-poor cell lines, in which Epac1 expression is lower than a half of Epac1 expression in SK-Mel-2 (HEMA-LP, WM3248, WM1552C, and WM115 cells). Conditioned medium (CM) of C8161 cells, which expresses abundant Epac1 (Baljinnyam et al., 2011), increased migration of human umbilical vein endothelial cells (HUVEC) (Figure 1A). Both a neutralizing antibody against FGF2 and heparitinase, a HS-cleaving enzyme, inhibited the CM-induced HUVEC migration. Knockdown of Epac1 in C8161 cells (Figure 1B) suppressed the CM-induced HUVEC migration (Figure 1A). Hence, these data suggested that Epac1 in melanoma cells can increase migration of endothelial cells via FGF2- and/or HS-dependent mechanisms.

### Epac1 in melanoma cells induces tube formation of endothelial cells via cell/cell communication

As endothelial cell migration is fundamental for angiogenesis (Lamalice et al., 2007), we examined whether Epac1-expressing melanoma cells can stimulate endothelial tube formation, which mimics *in vivo* angiogenesis. As shown in Figure 2A, B, CM of C8161 cells increased tube formation of HUVEC. Similar to migration (Figure 1A), the CM-induced tube formation was inhibited by the neutralizing antibody against FGF2 and by heparitinase. In addition, CM of C8161 cells in which Epac1 was knocked down showed reduced tube formation (Figure 2A, B). *In vivo* angiogenesis assay showed the same effect of Epac1 knockdown (Figure 2C, D). These data suggested that Epac1 in melanoma cells have the ability to induce angiogenesis via FGF2- and/or HS-mediated cell/cell communication.

### Epac1 in melanoma cells increases migration of neighboring melanoma cells via cell/cell communication

Based on the increased HUVEC cell migration shown previously, we hypothesized that a similar cell/cell interaction may also exist among melanoma cells. To test this hypothesis, we examined whether CM derived from a melanoma cell line affects migration of other melanocyte/

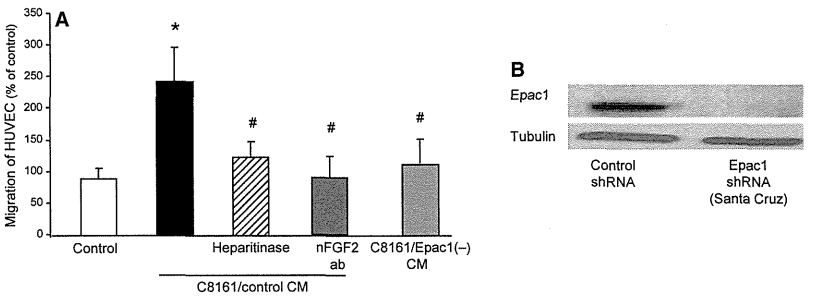


**Figure 1.** Epac1 in melanoma cells increases migration of endothelial cells via cell/cell communication. (A) CM of C8161 (C8161/control CM) increased migration of human umbilical vein endothelial cells (HUVEC). Epac1 knockdown in C8161 cells (C8161/Epac1(–) CM) inhibited the CM-induced migration. The CM-induced increase in migration was inhibited by the neutralizing antibody against FGF2 [nFGF2 ab (25 μg/ml)], and heparitinase (0.08 U/ml). *P < 0.05 versus control, #P < 0.05 versus C8161/control CM, n = 4. (B) Western blot of C8161 cells with stable knockdown of Epac1 performed with lentivirus-based shRNA induction.

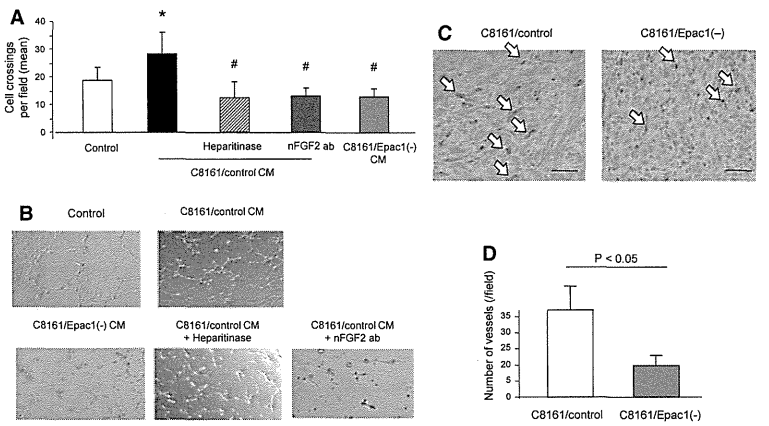


**Figure 2.** Epac1 in melanoma cells activates angiogenesis. (A) C8161/control CM increased tube formation of human umbilical vein endothelial cells (HUVEC). C8161/Epac1(–) CM showed reduced tube formation compared to C8161/control CM. The C8161/control CM-induced tube formation was inhibited by nFGF2 ab (25 μg/ml), and by heparitinase (0.08 U/ml). C8161/Epac1(–) CM showed reduced tube formation compared with C8161/control CM.*P < 0.01 versus control medium. #P < 0.01 versus C8161/control CM, n = 4. (B) Representative images of HUVEC tube formation described in A. (C and D) Epac1 knockdown reduces angiogenesis *in vivo*. C8161 cells with or without Epac1 knockdown ($1 \times 10^6$ cells) were inoculated in the interscapular region of BALB/c mice. One week after the inoculation, tumor was removed. (C) Immunohistochemical images with anti-CD31 staining for the detection of endothelial cells are shown. White arrows indicate CD31-positive cells stained brown. Scale bar: 100 μm. (D) The number of microvessels in each mouse was counted with the positively stained cells in 10 different fields, n = 4.

melanoma cells. CM from WM3248 or WM115 cells, both primary melanoma cell lines, did not change cell migration of HEMA-LP melanocyte cells (Figure 3A). In contrast, CM sourced from SK-Mel-2 or C8161 cells, both metastatic melanoma cell lines, increased migration of HEMA-LP. Migration of WM1552C cells, a primary melanoma cell line of the radial growth phase (RGP), was examined next (Figure 3B). CM of WM3248, a melanoma cell line of the vertical growth phase (VGP), SK-Mel-187, SK-Mel-2, or C8161 cells, all metastatic melanoma cell lines, increased WM1552C cell migration (Figure S3). In contrast, migration of the metastatic melanoma cell line, C8161 cells, was not affected by CM of SK-Mel-2. Epac1 overexpression (OE) in Epac1-poor melanoma cells indeed increased cell migration in both WM115 and WM3248 cells (Figure S1), suggesting that Epac1's effect on migration is saturated in Epac1-rich melanoma cells such as C8161 and SK-Mel-2 cells. Epac1 knockdown by two different Epac1 shRNAs (from Santa Cruz Biotechnology and Sigma Aldrich) in C8161 cells inhibited the CM-induced migration of HEMA-LP and WM1552C cells (Figure 3A, B and S2). Similar result was obtained in Epac1 knockdown in SK-Mel-2 cells (Figure 3B). These data suggested the specific role of Epac1 in the CM-induced migration.

The CM-induced migration of HEMA-LP and WM1552C cells were inhibited by heparitinase (Figure 3A and B), and the CM-induced migration of WM1552C cells was suppressed by the neutralizing FGF2 antibody (Figure 3B). The neutralizing FGF2 antibody inhibited CM-induced migration in other combinations of CM and cell lines used for migration (Figure S3). In addition, Epac1 OE in WM3248 cells increased their migration, and it was reduced by neutralizing FGF2 antibody (Figure S4).These

 

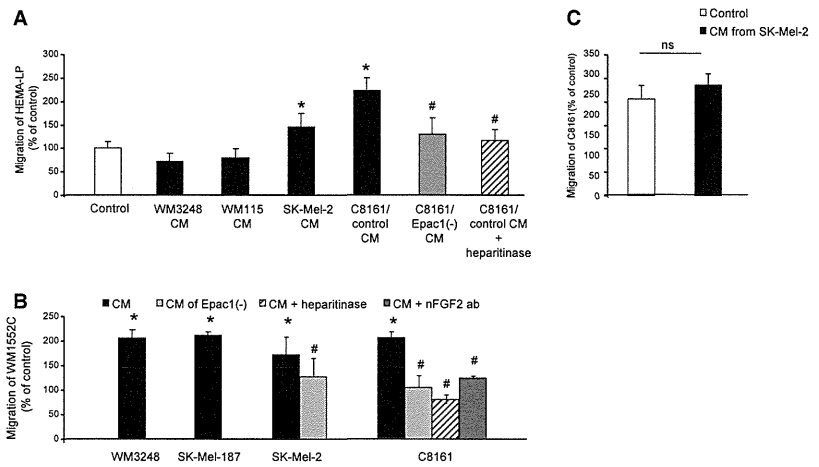


**Figure 3.** Epac1 in melanoma cells increases migration of melanocytes/other melanoma cells. (A) Conditioned media of indicated melanoma cell lines were used for the Boyden chamber migration assay of HEMA-LP cells. Conditioned media from SK-Mel-2 and C8161 cells, but not those from WM3248 and WM115 cells, increased migration of HEMA-LP cells. Knockdown of Epac1 (C8161/Epac1(−) CM) as well as heparitinase inhibited the CM-induced migration. *P < 0.05 versus control medium, #P < 0.05 versus C8161/control CM, n = 4. (B) Conditioned media of indicated melanoma cell lines were used for the Boyden chamber assay of WM1552C cells. Conditioned media of all cell lines examined increased migration of WM1552C cells. Knockdown of Epac1 inhibited migration induced by CM derived from SK-Mel-2 and C8161 cells. Heparitinase and the nFGF-2 antibody suppressed migration induced by CM of C8161 cells.*P < 0.05 versus control medium, #P < 0.05 versus CM, n = 4. (C) The Boyden chamber assay showed that CM of SK-Mel-2 cells did not increase migration of C8161 cells, n = 4.

data suggested that CM-induced migration was regulated by Epac1, HS and/or FGF2 signaling.

### Epac1 augments the binding of FGF2 to FGF receptor

We next investigated the effects of Epac1 on HS including N-sulfation and FGF2 signaling. It has been demonstrated that perlecan interacts with FGF2 via its HS chains (Knox et al., 2002; Sharma et al., 1998). We thus examined perlecan expression of CM by isolation with chromatography. N-sulfated HS chains of perlecan were detected by the anti-HS antibody (clone 10E4) (Figure 4A). The N-sulfation of HS bound to the perlecan was significantly reduced by Epac1 knockdown. In addition, both the amount of N-sulfation and the number of FGF receptors bound to FGF2 were decreased by knockdown of Epac1 (Figure 4B). In contrast, neither the expression of total HS bound to FGF2 nor FGF2 itself in CM were changed by Epac1 knockdown (Figure 4B), suggesting that Epac1 enhances FGF2-binding to FGF receptor via N-sulfation of HS. The binding assay showed that CM from C8161 cells increases FGF2 binding to FGF receptor expressed in HUVEC cells. The CM-induced FGF2 binding was inhibited by the FGF2 antibody and by Epac1 knockdown in C8161 cells (Figure 4C). Taken together, these data demonstrated that Epac1-expressing melanoma cells regulate paracrine-acting FGF2 signaling in neighboring cells such as endothelial and melanoma cells by modification of HS.

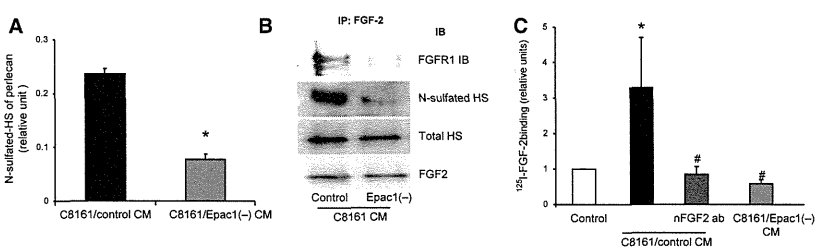


**Figure 4.** Epac1 enhances the binding of fibroblast growth factor (FGF2) to FGF receptor via N-sulfation of HS. (A) Perlecan was isolated from the DEAE chromatography fractions using a polyclonal antiperlecan antibody. The presence of HS chains on perlecan was detected using an anti-HS-specific antibody (10E4). Epac1 knockdown reduced the amount of N-sulfated HS attached to perlecan. *P < 0.05 versus C8161/control CM, n = 8. (B) CM of C8161 was subjected to immunoprecipitation with the antibody against FGF2 followed by Western blot for indicated antibodies. Both N-sulfated HS and FGF receptor 1 (FGFR1) attached to FGF2 were reduced by Epac1 knockdown whereas the amount of FGF2 in the CM was not different. (C) The binding assay for FGF2 in human umbilical vein endothelial cells (HUVEC) was performed with indicated CM. C8161/control CM increased the binding of FGF2 to HUVEC. The neutralizing antibody for FGF2 (nFGF2 ab) and knockdown of Epac1 inhibited the CM-induced FGF2 binding. *P < 0.05 versus control medium, #P < 0.05 versus C8161/control CM, n = 4.

### Epac1-rich melanoma cells support proliferation of Epac1-poor melanoma cells *in vivo*

Increased angiogenesis by Epac1 (Figure 2) suggested that Epac1-rich melanoma cells can support proliferation not only of Epac1-rich melanoma cells themselves but also of Epac1-poor melanoma cells via newly supplied blood flow. If this is the case, melanoma cells expressing low Epac1 that cannot survive *in vivo* are rescued by coexistence of Epac1-rich melanoma cells. Therefore, we examined whether coinoculation of melanoma cells with high Epac1 expression and those with low Epac1 expression enables the second type of cells to survive in mice. To show this, we used SK-Mel-2 cells, which abundantly express Epac1, and WM1552C cells, which poorly express Epac1 (Baljinnyam et al., 2011). In addition, we used green fluorescent protein (GFP) – or red fluorescent protein (RFP) to distinguish WM1552C cells from SK-Mel-2 cells. Our study showed that SK-Mel-2 cells inoculated in athymic nude mice, but not WM1552C cells, formed a tumor (Figure 5A), suggesting that WM1552C cells alone cannot survive in mice. A tumor was formed by WM1552C cells coinoculated with SK-Mel-2 cells, but not with WM1552C cells inoculated alone (Figure 5A–C). The tumor formed by the coinoculation showed both GFP- and RFP-fluorescent signal (Figure 5D). In addition, fluorescence-activated cell sorting (FACS) analysis demonstrated that individual cells isolated from the tumor have either RFP signal or GFP signal (Table 1). These data showed the existence of both WM1552C and SK-Mel-2 cells in the tumor and thus suggested that Epac1-rich melanoma cells can support the survival of Epac1-poor melanoma cells. As the percentages of GFP- and RFP-positive cells are not equal even in the same SK-Mel-2 cells (Table 1) under *in vivo* conditions, it seems that one of the two inoculated cell lines becomes dominant. As CM of SK-Mel-2 cells did not increase proliferation of WM1552C cells (data not shown), these data suggest that SK-Mel-2 cells enable WM-1552C to survive *in vivo* most probably by modification of the extracellular matrix and enhanced angiogenesis.

## Discussion

Our previous reports showed that Epac1 increases migration of melanoma cells themselves (Baljinnyam et al., 2009, 2010, 2011). Epac1 in melanoma cells may regulate the cell–cell communication, which could lead to an augmented migration of neighboring endothelial and melanoma cells. Our findings suggest that Epac1-rich melanoma cells play a major role in melanoma progression through migration of the Epac1-rich melanoma cells themselves, but also through increasing migration of neighboring Epac1-poor melanoma cells and more importantly, by the increased migration of neighboring endothelial cells that can accelerate tumor growth via angiogenesis. Therefore, it is plausible that Epac1-rich population in the melanoma tumor critically regulates tumor growth rate.

Although a number of reports demonstrated the role of FGF2 in melanoma progression (Gartside et al., 2009; Hibino et al., 2005; Meier et al., 2000; Ozen et al., 2004), little attention was focused on the role of paracrine-acting FGF2. Using B16F10, an invasive mouse melanoma cell line, CM-activated capillary formation of bovine aortic endothelial cells (Garrido et al., 1995). CM from A375, a

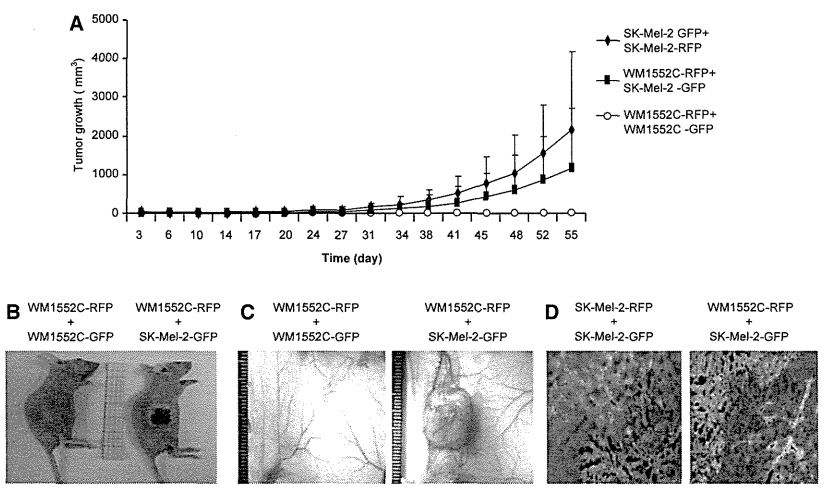


**Figure 5.** Epac1-rich melanoma cells support survival of Epac1-poor melanoma cells. (A) Tumor growth of WM1552C and SK-Mel-2 cells expressing Red Fluorescent Protein (RFP) and Green Fluorescent Protein (GFP) is shown. A mixture of indicated cells was injected in the right dorsolateral flank region in athymic BALB/c nude mice. Tumor size was measured twice a week to calculate tumor volume. Tumor failed to grow in the mixture of RFP- and GFP-labeled WM1552C. (B and C) Representative images of the tumors in the 12 weeks after the inoculation are shown. The mixture of RFP-labeled WM1552C cells and GFP-labeled SK-Mel-2 cells formed a tumor. (D) Representative images of coimmunostaining for RFP and GFP of the tumors formed by the indicated cell mixtures. Blue indicates 6-diamidino-2-phenylindole (DAPI) staining.

**Table 1.** Fluorescence activated cell sorting (FACS) analyses for the population of red fluorescent protein (RFP)- and green fluorescent protein (GFP)-positive cells in melanoma tumor

| Cell lines coinoculated | Fluorescent signal used | % of total sorted cells in tumor | SD |
|---|---|---|---|
| WM1552C-RFP + SK-Mel-2-GFP | RFP | 0.26 | 0.21 |
| | GFP | 85.9 | 4.72 |
| SK-Mel-2-RFP + SK-Mel-2-GFP | RFP | 3.22 | 1.8 |
| | GFP | 42 | 1.6 |

Formed tumors with coinoculation of indicated cell lines were isolated, dissected, and subjected to FACS analyses, n = 4.

human melanoma cell line, but not from normal melanocytes, increased migration and invasion of human mesenchymal stem cells. The CM-induced migration was inhibited by neutralization of FGF2 (Watts and Cui, 2012). Our results are consistent with these studies showing that CM of human melanoma cells increased migration of human endothelial cells via FGF2 signaling (Fig. 1). Furthermore, we have demonstrated the role of Epac1 in migration of endothelial cells via paracrine-acting FGF2 signaling, which subsequently results in increased angiogenesis (Figure 2). In addition, our results indicated the existence of FGF2-dependent cell/cell communication not only between melanoma and endothelial cells but also between melanoma and melanoma cells. This melanoma/melanoma cell communication in migration was obvious between Epac1-rich and Epac1-poor melanoma cells, but unclear between Epac1-rich and Epac1-rich melanoma cells (Figure 3C). This lacking of cell/cell communication is probably explained by saturated migration via abundant expression of Epac1 in the same cells as we have previously shown (Baljinnyam et al., 2011) and by the minimal effect of autocrine FGF2 signaling. Regarding WM1552C migration (Figure 3B), although Epac1's expression varies between the cell lines used for the study, the degree of migration did not directly reflect the degree of Epac1 expression. This was attributable, at least in part, to saturation of paracrine-acting FGF2 signaling and is supported by the data showing that FGF2 receptor expression is much higher in WM1552C cells compared with HEMA-LP (data not shown) in which the effects of CM are variable. Altogether, in terms of melanoma progression, Epac1's role in migration affects three types of cells: 1) Epac1-rich melanoma cells themselves, 2) Neighboring endothelial cells, 3) Neighboring Epac1-poor melanoma cells. Accordingly, targeting Epac1 would be an inhibitory mechanism for melanoma progression.

Perlecan is necessary for the binding of FGF2 to FGF receptor in human melanoma cells (Aviezer et al., 1997). N-sulfation of HS chains is critical for this interaction (Faham et al., 1996; Kreuger et al., 1999; Maccarana et al., 1993; Schlessinger et al., 2000). Although N-sulfation is largely regulated by NDSTs, little is known about how the expression/activity of NDSTs is regulated. We have shown that Epac1 can increase NDST-1 expression in melanoma cells (Baljinnyam et al., 2009). In addition, N-sulfation of HS was increased in the mixture of medium and cell lysate (Baljinnyam et al., 2011). In the present study, N-sulfation of secreted perlecan in the CM was reduced by Epac1 knockdown (Figure 4A). Furthermore, FGF2 binding to FGF receptor was inhibited by Epac1 knockdown (Figure 4B, C). Therefore, it is proposed that Epac1-rich melanoma cells can affect FGF2 signaling in neighboring cells via modification of N-sulfation of HS on perlecan. Meanwhile, knockdown of Epac1 reduced the amount of perlecan as demonstrated by Western blot analysis with a perlecan-specific antibody (CCN-1) (data not shown). Interestingly, expression of perlecan is regulated by the cAMP response element (CRE) as its promoter (Furuta et al., 2000). Thus, Epac1 potentially may regulate perlecan expression itself in addition to N-sulfation of HS, suggesting multiple roles of Epac1 on biosynthesis HSPG. However, further studies would be required to confirm this because another study found that Epac1 does not regulate transcription through CREB transcription factors and that the best characterized route for Epac1 to regulate transcription is through C/EBP transcription factors (Yarwood et al., 2008, JBC).

Our data showed that melanomas formed by coinoculation of Epac1-rich and Epac1-poor melanoma cells involved both melanoma populations (Figure 5D and Table 1). These data suggest that cell/cell communication within melanomas may support the survival of melanoma cells with lower malignancy potential. To confirm that Epac1 in Epac1-rich melanoma cells affect proliferation of another Epac1-poor melanoma cells, it is necessary to examine whether Epac1 knockdown decreases the number of Epac1-poor melanoma cells *in vivo*. However, inhibition of Epac1 itself affects angiogenesis as shown in our data (Figure 2), which may result in decreased proliferation of Epac1-rich (SK-Mel-2) cells themselves. Indeed, knockdown of Epac1 reduced tumor growth *in vivo* (data not shown). Therefore, knockdown of Epac1 itself may affect the local blood supply and thus survival and proliferation of Epac1-poor melanoma cells. Therefore, when Epac1 is knocked down in Epac1-rich melanoma cells, multiple factors may affect proliferation of Epac1-poor melanoma cell, suggesting difficulty of interpretation of the acquired data. Recently, specific Epac1 inhibitors have become commercially available. These inhibitors, HJC-0350 and ESI-09, indeed suppressed CM-induced migration in WM3248 cells (Figure S5), suggesting potential usage of these inhibitors for melanoma therapy, which will be addressed in our future study. Finally, HS binds to and regulates the activity of extracellular superoxide dismutase (EC-SOD), which results in increased protection against oxidative stress (Yamamoto et al., 2000). In addition, a device containing HS to deliver FGF2 enhanced FGF2's antioxidative property (Galderisi

et al., 2013). Accordingly, one could argue that Epac1 has antioxidative stress effects via the modification of HS-FGF2 signaling. Indeed, CM of SK-Mel-2 cells inhibited $H_2O_2$-induced apoptosis of WM1552C cells (data not shown). This antiapoptotic effect of the CM may modify the survival of WM1552C cells coinoculated with SK-Mel-2 cells *in vivo* (Figure 5), whereas rigorous examination for the protection against antioxidative stress should be performed to obtain conclusive evidence.

In summary, this study for the first time demonstrated Epac1-mediated cell/cell communication by modification of FGF2–HS interaction. Our findings may lead to a new strategy for the melanoma therapy targeting a certain population of melanoma cells, that is, Epac1-rich melanoma cells. Future research should attempt to examine the effect of Epac1-specific inhibitors on melanoma progression.

## Methods

### Reagents and cell lines

HEMA-LP was purchased from Invitrogen (Carlsbad, CA, USA), HUVEC was from VEC Technologies. WM1552C was from Dr. Meenhard Herlyn, Wistar Institute. C8161 cell line was provided by Dr. Mary JC Hendrix. SK-Mel-2 cells (ATCC) were maintained in MEM containing 10% FBS, 1% penicillin/streptomycin. WM1552C and C8161 cells were maintained in RPMI with 10% FBS, 1% penicillin/streptomycin. HEMA-LP and HUVEC cells were maintained in EndoGRO medium (EMD Millipore, Billerica, MA, USA) containing 5% FBS. Antibodies against Epac1, FGF2, and FGFR-1 were from Cell Signaling, anti-NDST-1 antibody was from Abnova and anti-α-tubulin antibody was purchased from Abcam (Cambridge, MA, USA).

### Short hairpin RNA transduction

Short hairpin RNA (shRNA) transductions with lentivirus (Santa Cruz Biotechnology) were performed as we previously described (Baljinnyam et al., 2010). C8161 cells were incubated with 8 μg/ml of Polybrene and lentiviral particles harboring shRNA were selected with puromycin dihydrochloride for 1 week. Fresh puromycin-containing medium was replaced every 3–4 days. Established cell lines are as follows: C8161 cells with control shRNA (C8161/control), C8161 cells with Epac1 shRNA [C8161/Epac1(−)].

### Migration assay

Migration assay was performed using the 24-well Boyden chambers (8 μm pores, BD Biosciences, San Jose, CA, USA) as we previously described (Baljinnyam et al., 2009). The cells were plated at a density of $1 \times 10^6$ cells/100 μl of medium in the inserts and incubated for 16 h at 37°C in the conditioned media. The insert membranes were stained using the Diff-Quick kit (Dade Behring). Pictures were taken and migrated cells were counted with Image J software using 10 randomly chosen fields.

### Purification of human perlecan

About 2 L of conditioned medium for 72 h by confluent cultures of human melanoma cells was purified by DEAE–Sepharose chromatography (Whitelock et al., 1999) (100 ml bed volume, flow rate 1 ml/min) which had been equilibrated with 250 mM NaCl (20 mM Tris, 10 mM Methylenediaminetetraacetic acid, 1 mM phenylmethylsulfonyl fluoride, 1 mM benzamidine, pH 7.5). The column was washed extensively with the buffer, and bound proteins were eluted using 1 M NaCl, 20 mM Tris, 10 mM Methylenediaminetetraacetic acid. The presence of HS-bound perlecan was monitored in column fractions using antibodies to HS (10E4) in an enzyme-linked immunosorbent assay (ELISA). The protein concentration was measured using the Coomassie Plus assay (Pierce), and aliquots were stored at −70°C until used for further Western blot analyses.

### Western blot analysis

Western blot analysis was performed as previously described (Iwatsubo et al., 2003, 2004). Briefly, cells were lysed and sonicated in RIPA lysis buffer. Equal amounts of protein were subjected to SDS-PAGE, were transferred to Millipore Immobilon-P membrane, and immunoblotting with respective antibodies was performed.

### Tube formation assay

Human umbilical vein endothelial cells under seven passages were used in all experiments. *In vitro* angiogenesis tube formation assay was performed as we previously described with some modifications (De Lorenzo et al., 2004; Movafagh et al., 2006). HUVEC (5000/well) were seeded in 24-well plates coated with Matrigel (Biosciences Discovery), incubated in CM for 4 h at 37°C. The tube formation was quantified by counting the number of connecting branches between two discrete endothelial cells.

### Immunoprecipitation

Dynabeads-Protein G for immunoprecipitation (Life Technologies, Carlsbad, CA, USA) were incubated with the primary antibodies and added to the soluble cell lysate fraction. These antibody-coated Dynabeads™, Life Technologies, Carlsbad, CA, USA bound to the target proteins were separated by the magnet and after repeated washing three times, the isolated protein complexes were subjected to SDS-PAGE and immunoblotting with respective antibodies.

### FGF2-binding assay

FGF2-binding assay was performed as previously described (Reiland and Rapraeger, 1993). Briefly, HUVEC cells were plated in 24-well plate with $1.5 \times 10^5$ cells

 